12-2012

STUDY ON CORROSION ACTIVITY OF CARBON STEEL IN CONCRETE SIMULATED PORE SOLUTION UNDER STATIC TENSILE AND COMPRESSIVE STRESSES

Yujie Zhang
Clemson University, silvia101jing@gmail.com

STUDY ON CORROSION ACTIVITY OF CARBON STEEL IN CONCRETE SIMULATED PORE SOLUTION UNDER STATIC TENSILE AND COMPRESSIVE STRESSES

A Thesis
Presented to
the Graduate School of
Clemson University

In Partial Fulfillment
of the Requirements for the Degree
Master of Science
Civil Engineering

---

by
Yujie Zhang
December 2012

Accepted by:
Dr. Amir Poursaee, Committee Chair
Dr. Prasad Rao Rangaraju
Dr. Bradley J. Putman

ABSTRACT

Reinforced concrete is a structure material made up of concrete with relatively lower tensile strength containing reinforcements with higher tensile strength and better ductility, which are embedded into fresh concrete to resist tensile stress in certain regions of concrete. Steel reinforced concrete is most widely used around the world in civil engineering structures, water conservancy and highway construction due to its durability strength and reasonable cost.

However, reinforced concrete structures such as bridges and parking lots slabs inevitably experience variable loads and constant degradation from the aggressive environments, such as marine and deicing salts. Therefore, it is imperative to study the synergic impact of different types of loadings and exposure to chloride ions on the corrosion of steel rebars. Clear understanding of such processes assists improving the resiliency of the structures and helps extending the service life of the constructions by modifying the design codes of structural steel, which will thus improve the durability and safety of next generation of sustainable infrastructures. In addition, it is necessary to understand the fundamental mechanism of steel passivation and depassivation processes in concrete under stresses, then more reliable and robust service life modeling tools can be made to help engineers predict the state and performance of rebar in concrete structures.

Hence, in order to obtain detailed understanding of the effect of both tensile and compressive stresses on passive film and the depassivation process, experiments were

performed on steel immersed in concrete simulated pore solution under different types and degrees of loadings. Simulated concrete pore solution was chosen in order to obtain the results in a reasonable time frame required for this project. Several electrochemical measurement techniques were used. Besides, Mott-Schottky technique was utilized to investigate the semi-conductive behavior of the passive film, which is formed on the surface of the steel rebars. Results indicate that steel specimens in chloride free pore solution under tensile loadings passivate more rapidly compared to those under compressive loadings. However, the situation in chloride contaminated solution is different and steel under tensile stress exhibit more corrosion than that under compressive stress and no load.

DEDICATION

This thesis is dedicated to my mother Xiuzhen Yang, my father- Cheng Zhang, and my husband Peng Wu. Their love has always encouraged and protected me through my life.

ACKNOWLEDGMENTS

First of all, I would like to express my sincere gratitude to my major advisor, Dr. Amir Poursaee for his invaluable advices, encouragements, and inspirations. Without his elaborate guidance and persistent help, this thesis would not have been possible.

I also appreciate the help from my committee members Dr. Bradley Putman and Dr. Prasad Rao Rangaraju, not only for their work on this thesis but also for everything they did in research and coursework through my one and half year in Clemson University.

Finally, I would like to thank my parents and family. They always understand and support me with a lot of patience, no matter where I am and what I am doing. They are the power of my study.

In addition, I would like to acknowledge the following individuals for their helpful contributions, without which this work would have been impossible:

Arash Razmjoo	Sami Pant	Danny Metz
Fangqian Liu	Yuanchao Feng	Matthew Adamson
Huan Sheng		

TABLE OF CONTENTS

Page

Table of Contents (Continued)

Page

LIST OF TABLES

Table Page

LIST OF FIGURES

List of Figures (Continued)

Figure Page

CHAPTER ONE

1. INTRODUCTION AND LITERATURE REVIEW

1.1 Introduction

Reinforced concrete is a structural material made up of concrete with relatively lower tensile strength containing reinforcements with higher tensile strength and better ductility, which are embedded into fresh concrete to resist tensile stress in concrete. With the development of material engineering, concrete can contain various fiber reinforcements like polymer, steel and other composite material, among which steel reinforced concrete is most widely used around the world in civil engineering, water conservancy and highway construction due to its excellent mechanical strength and reasonable cost.

In practice, safety and durability is one of the most critical issues for the reinforced concrete structures, however, corrosion of steel bars in concrete could lead to critical damage, even casualties to concrete. It is reported that the annual direct cost of corrosion in the US is estimated at $22.6 billion and keeps increasing [1], in which the corrosion of steel in concrete takes a significant portion. According to the Federal Highway Administration (FHWA) the estimated cost through 2011 of corrosion protection of concrete bridges maintenance was $5.2 billion [2]. Therefore the durability issue due to rebar corrosion in concrete has drawn more and more worldwide attention. Factors inducing corrosion of steel can be aggressive environment like acid rain or

deicing salts, or various loadings that reinforced concrete structures such as bridges and parking lots slabs always experience. Many studies have been performed on the corrosion of steel rebars exposed to different deicing salts [3-5]. However, no research on the effect of different loadings on the corrosion behavior of the steel bars in concrete or concrete simulated environment has been found. Therefore, it is imperative to study the impact of different loadings on the corrosion of steel in concrete environment.

1.2 Literature review

1.2.1 Concrete nature

Concrete is a composite material composed of coarse and fine granular material (the aggregate or filler) embedded in a hard matrix of material (the cement of binder) that fills the space between the aggregate particles and glues them together. Aggregates and cement can be manufactured from many diverse chemicals. Portland cement concrete, the most widely used concrete, contains fine and coarse aggregate and portland cement paste, which mainly consists of calcium silicates (C_3S and C_2S), calcium aluminate (C_3A), iron-containing clinker phase (C_4AF) and other compounds [6]. Pores within the concrete, filled with saturated $Ca(OH)_2$ solution, and other alkalines such as NaOH and KOH [7] which provide very high pH to the concrete environment. Typical concrete mixtures have high compressive strength (about 35MPa (5000psi)) [8], but relatively low tensile strength which may cause the microscopic rigid structure to break, resulting in cracking

and separation of the concrete [9]. For this reason, typical non-reinforced concrete must be well supported to prevent the development of tension. If a material with high strength in tension, such as steel, is placed in concrete, then the composite material, reinforced concrete, resists not only compression but also bending and other direct tensile actions [10].

1.2.2 Passivation of steel in concrete

Steel's nature is tending to undergo corrosion reactions; the alkaline environment of concrete (pH of 12 to 13) provides both physical and chemical protection to reinforcing steel bars by its cover and high pH environment. At the high pH, a thin oxide layer, passive film, forms on the steel and prevents metal atoms from dissolving. This passive film does not actually stop corrosion; it reduces the corrosion rate to an insignificant level. For steel in concrete, the passive corrosion rate is typically10^{-4} to 10^{-3} A/m^2 [13] .Without the passive film, the steel might corrode at rates of 1,000 times higher than that in its passive state [14]. As seen in Figure 1-1, the Pourbaix diagram [15] defines the range of electrochemical potential and pH for Fe-H_2O system in alkaline environment, in which blue box shows typical values of potentials and pH levels for reinforcing steel. The steel remains passive within concrete's potential and pH range, where a passive layer forms on the surface of steel, with thickness less than 10nm [16]. Previous research indicated that the protectiveness of passive film increases when steels are exposed in alkaline solutions [17,18]. However steel bars do get corrosion in field, where concrete cannot provide permanent protection. This passive film remains on steel

when pH value of pore solution is between 10 and 13 and would breakdown when the pH value is below 10 [19]. Corrosion initiates with the breakdown of the passive film, known as depassivation. Corrosion products are thus formed on the steel bars which are expansive, as seen in Figure 1-2 [20]. It was confirmed that iron exists in three oxidation states in the passive films: Fe^{0}, Fe^{2+} and FeOOH in alkaline environment without aggressive species [21]. The corrosion products can cause cracking, weakening the concrete, decreasing safety and durability of the infrastructure.

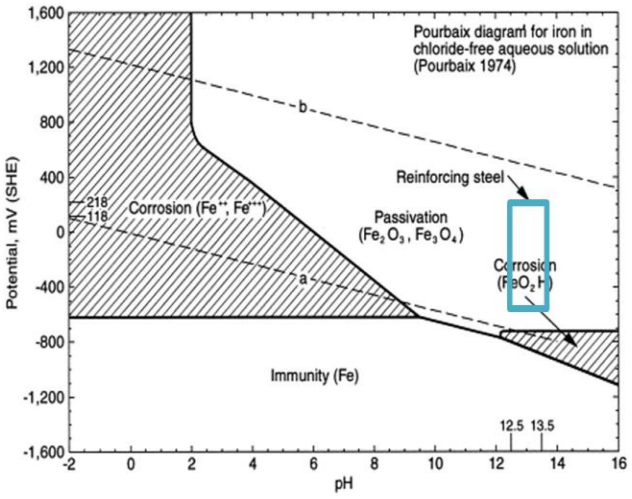

Figure 1-1. Pourbaix diagram for iron in a chloride-free aqueous solution.

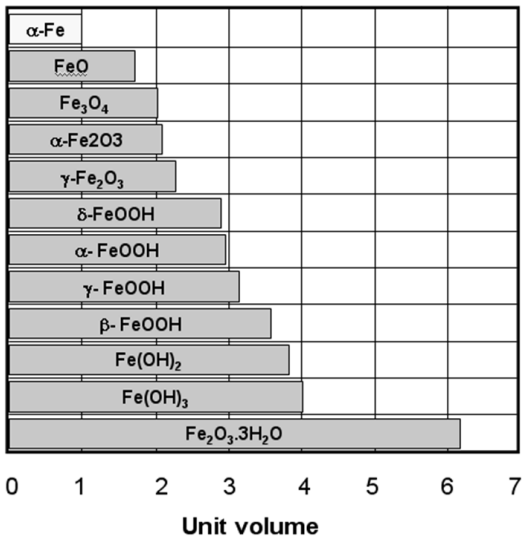

Figure 1-2. Unit volume of iron corrosion products.

1.2.3. Electronic behavior of passive film

Due to the nature of the passive films on metals, they usually show electrochemical properties of a semiconductor. The properties of semiconductive electrodes and their differences from those of metallic electrodes can be understood by investigating the electronic structures of these materials [22]. In this investigation, essentially infinite number of atoms must be considered. Therefore, the electronic structure of these solids is usually discussed in terms of energy bands, which are made up of the atomic orbitals. The highest and lowest energy levels of a band are referred to as the band edges. The highest occupied level, called the valence band, and the lowest unoccupied, called the conduction band, are of interest. The energy gap (the band gap) between these bands (i.e., the difference in energy between the upper edge of the valence

band and the lower edge of the conduction band) determines the properties of the material. Conductivity of a solid state material requires that the electrons occupy partially filled orbitals. This is achieved by occupancy of the conduction band. As can be seen in Figure 1-3 [22], for metals, the conduction and valence bands overlap, so the conduction band can be readily occupied. For insulators, the band gap is large and electrons cannot be promoted from the valence band to the conduction band. However, for semiconductors, the band gap is not as large, and electrons can be moved into the conduction band.

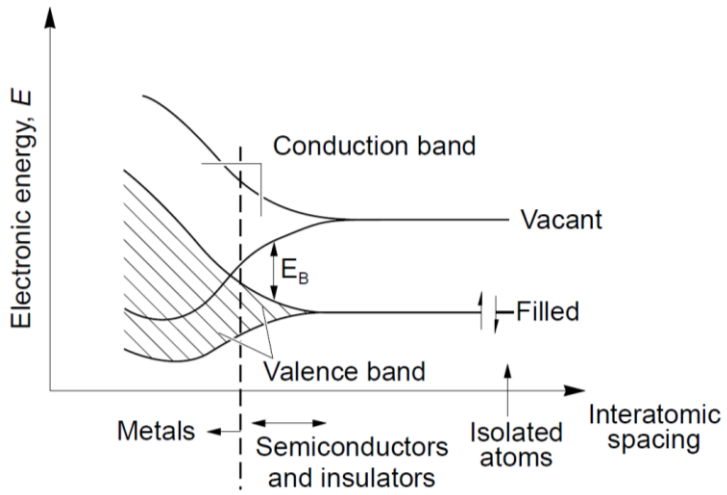

Figure 1-3. Generation of bands in solids from atomic orbitals of isolated atoms

The movement of electrons leaves a positively charged vacancy in the valence, which is referred to as a hole [23]. Holes are considered to be mobile, because they can be moved through space by the transfer of an electron to the vacancy. Thus they also cause conduction. Electrons can be excited to the conduction band either thermally or

photochemically. Nevertheless, there is another method for generating charge carriers (using electrons or holes) within a semiconductor, called doping, which involves the addition of a different element, dopant, into the semiconductor [23]. An example of this is the introduction of a group V element (e.g., P) or a group III element (e.g., Al) into a group IV element (e.g., Si) in the periodic table. The addition of P into Si introduces occupied energy levels into the band gap close to the lower edge of the conduction band and the addition of Al introduces vacant energy levels into the band gap close to the upper edge of the valence band. Therefore, the addition of the P to Si allows easy promotion of electrons into the conduction band while the addition of Al leads to the formation of holes in the valence band. Undoped semiconductors are referred to as intrinsic semiconductors. Doped semiconductors in which the majority of charge carriers are electrons are referred to as n-type semiconductors, whereas those in which holes are the majority charge carriers are referred to as p-type semiconductors.

As aforementioned, the generation of charge carriers requires the presence of dopants. The dopants must be able to give off electrons to the conduction band in which case they are called donors or that they give off holes to the valence band in which case they are called acceptors (since they effectively accept an electron from the filled valence band). The donors provide free electrons to n-type semiconductors while acceptors provide free holes to p-type semiconductors.

The Fermi level is another important concept in discussion of solid state materials and semiconductors. The Fermi level is defined as the energy level at which the probability of occupation by an electron is 50%. For an intrinsic semiconductor the

Fermi level lies at the mid-point of the band gap. Doping changes the distribution of electrons within the solid, and consequently changes the Fermi level. For an n-type semiconductor, the Fermi level lays just below the conduction band, while for a p-type semiconductor it lays just above the valence band [22,23].

When a semiconductor contacts an electrolyte, charges are transferred between the semiconductor phase and the solution phase. In order for the two phases to be in equilibrium, their electrochemical potential must be the same.

The electrochemical potential of the solution is determined by the redox potential [24] [1] of the electrolyte solution, and the redox potential of the semiconductor is determined by the Fermi level. If the redox potential of the solution and the Fermi level do not lay at the same energy, a movement of charge between the semiconductor and the solution is required in order to equilibrate the two phases.

For a metallic electrode, the excess charge lays at the surface. However, for a semiconductor this charge extends into the electrode for a significant distance [23]. This region is referred to as the space charge region, and an electrical field is associated with it. Therefore, there are two double layers taken into account: the interfacial (electrode/electrolyte) double layer, and the space charge double layer (C_{sc}). For an n-type semiconductor electrode at open circuit potential (steady state condition), the Fermi level is usually higher than the redox potential of the electrolyte. Consequently electrons will be transferred from the electrode into the solution and there is a positive charge

[1] Redox reactions include all electrochemical reactions in which atoms have their oxidation state changed. The term comes from the two concepts of reduction and oxidation.

associated with the space charge region. The majority charge carrier of the semiconductor has been removed from this region. Therefore, this region is referred to as a depletion layer. For a p-type semiconductor, the Fermi level is generally lower than the redox potential, and hence electrons transfer from the solution to the electrode to reach equilibrium. This causes a negative charge in the space charge region. Since the holes in the space charge region are removed by this process, this region is also called a depletion layer. At a certain potential, the Fermi level lays at the same energy as the solution redox potential. There is no net transfer of charge, hence there is no band bending. This potential is referred to as the flatband potential, E_{fb}. E_{fb} plays the same role as the potential of zero charge for metals.

The surplus charges of the semiconductor phase are distributed in the space charge-layer. The charge distribution at the interface between a semiconductor and an electrolyte is often determined by measuring the capacitance of the C_{SC} as a function of the electrode potential (E). When the space charge double layer serves as a depletion layer, the relation of the capacitance and the potential conforms to the Mott-Schottky equation [23,25]

$$\frac{\mathbf{1}}{\mathbf{C_{sc}^2}} = \frac{\mathbf{2}}{\boldsymbol{\varepsilon\varepsilon_0 qN}}\left(\mathbf{E} - \mathbf{E_{fb}} - \frac{\mathbf{kT}}{\mathbf{q}}\right) \qquad \text{Equation 1-1}$$

The M-S relationship ($1/C_{sc}^2$ vs E plot) expresses the potential dependence of C_{SC} of a semiconductor electrode under depletion conditions, where N represents the donor (N_D) or acceptor density (N_A), ε is the dielectric constant of the passive film, ε_0 is the

vacuum permittivity (8.85×10^{-14} F/cm), q is electron charge (+e for electron, −e for vacancy, e=1.602×10^{-19} C), E_{fb} is the flat band potential, k is the Boltzmann constant (k=1.38×10^{-23} J/K) and T is the absolute temperature (kT/q is only about 25 mV at the ambient temperature and is assumed to be negligible). N_D and N_A can be determined from the slope of the experimental $1/C_{sc}^2$ vs E plots, while E_{fb} comes from the extrapolation for $1/C_{sc}^2$ =0. Mott-Schottky plots are shown for a p-type silicon semiconductor and an n-type silicon semiconductor in Figure 1-4 [26].

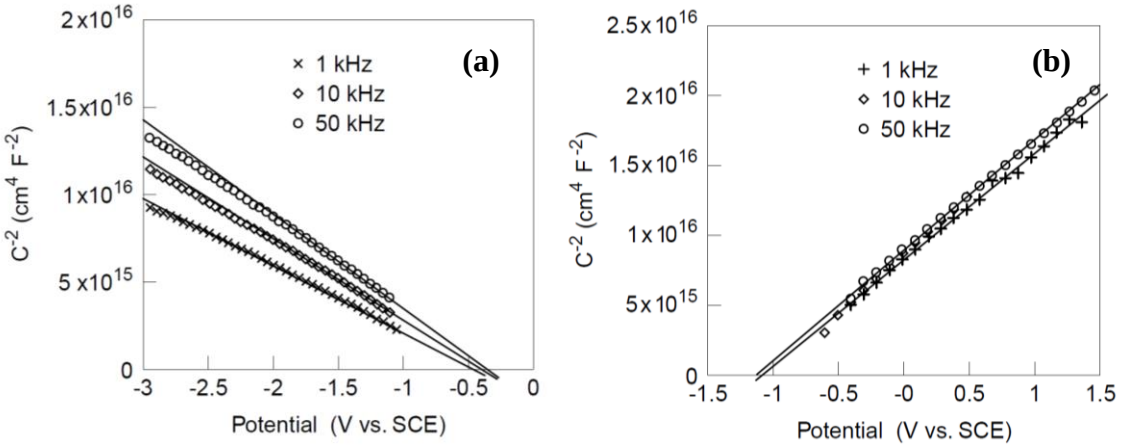

Figure 1-4. Mott-Schottky plots: (a) a p-type semiconductor, and (b) an n-type semiconductor

Characteristics and the role of passive films on Fe base metal and alloys have been one of the most important topics in the corrosion science. In general, passive film on the surface of steel could be interpreted in terms of a semiconductive film [27-32]. Therefore, the electronic properties should play an important role in the corrosion

resistance. However, much attention has been paid on the chemical composition and the microstructure of passive films [33,34].

Mott-Schottky analysis has been successfully used to investigate the semiconductive properties of passive films on metals. The type of the semiconductor, donor density (N_D) and the flat band potential (E_{fb}) can be obtained, using the Mott-Schottky plots [27,28,30,35-37].

1.2.4. Corrosion of steel in concrete

When rebar corrodes, the corrosion products expand intensively and will result in cracking in concrete and debonding between rebar and concrete. Corrosion of steel in concrete is an electrochemical process; the two most common conditions inducing rebar corrosion and breakdown of passive film in reinforced concrete are carbonation and chloride erosion [39]. Corrosion due to chloride attack is the main reason of corrosion of the steel rebars embedded in concrete in North America and is discussed further in the following section.

1.2.4.1. Chloride attack corrosion

When chloride ions coexist in concrete with other anions (OH^-), chloride ions are easier to be absorbed than OH^-, resulting in a much lower OH^- concentration near passive film than that in micro pores. This local reduction of pH value may initiate

localized breakdown of the film [40,41] .Besides, chloride atom is relatively small in radius but highly reactive, making it possible to break down the passive film and react with Fe atoms, forming an active-passive galvanic cell [39].

The corrosion reaction takes place with presence of water and oxygen as following [42]:

$$\text{Anode reaction:} \quad Fe^{2+} + 2e \rightarrow Fe$$

$$\text{Cathode reaction:} \quad O_2 + 2H_2O + 4e \rightarrow 4OH^-$$

The whole corrosion process is a combination of cathodic and anodic reaction, precipitating ferric hydroxide (rust) on the surface of steel bar, where $Fe(OH)_3$ will later turn into $nFe_2O_3 \cdot mH_2O$ (brown rust), leaving some incomplete oxidation products Fe_3O_4 (black rust) [43].

$$2Fe + 2H_2O \rightarrow 2Fe^{2+} + 4OH^- \rightarrow 2Fe(OH)_2$$

$$4Fe(OH)_2 + O_2 + 2H_2O \rightarrow 4Fe(OH)_3$$

The risk of corrosion increases as the chloride content of concrete increases, and the passive film is damaged and corrosion initiated when water and oxygen are available and the chloride ions concentration reaches a certain value, which is called the chloride threshold value [44]. Saremi et al [45] determined the threshold ratio of $[Cl^-]/[OH^-] = 0.6$ in simulated pore solution, above which the passive film became less resistant to

corrosion. Later Zhang's study indicated that the corrosion resistance and thickness of passive film would decrease when chloride ions (wt%<0.2%) exist in the solution, leading to breakdown of the passive films [46]. FHWA studies found that a threshold limit of 0.2% total (acid-soluble) chloride by weight of cement could induce corrosion of reinforcing steel in bridge decks [47]. However, only water-soluble chlorides promote corrosion; some acid-soluble chlorides may be bound within aggregates and, therefore, unavailable to promote corrosion. Study performed by the FHWA [48] found that the conversion factor from acid-soluble to water-soluble chlorides could range from 0.35 to 0.90, depending on the constituents and history of the concrete. Arbitrarily, 0.75 was chosen, resulting in a water-soluble chloride limit of 0.15 % by weight of cement.

Although much work were done on chloride attack, the mechanism of local breakdown of passive film by chloride ions is still not clear, mainly due to the difficulty of examination over the ultra-thin film and observation inside concrete.

1.2.5. Effect of loadings on passivation

As discussed above, passivation can be affected by several factors such as: pH value, chloride concentration and cement composition. Being one of the most common engineering structure materials, reinforcement also experience different kinds of loadings which might also have impact on the passivation/depassivation behavior.

A galvanic cell is formed when two dissimilar metals are electrically connected and a corrosion process is resulted. In other cases, one metal or two similar metals

immersed in same solution can also form a galvanic cell [24,49]. The electrical behavior of AA2024-T3 steel under tensile stress in 1M NaCl solution electrolyte was studied. The stressed sample was anodic versus the unstressed sample [50], and it was found that breakdown potential and current are higher for stressed samples than unstressed ones. Navai investigated the influence of the tensile and compressive stresses on the composition and thickness of the passive films formed on 302 stainless steel in a normal sulfuric acid solution, where a U-bend sample was used to simulate the effect of tensile and compressive stresses. It was concluded that tensile stress caused more oxidation than compressive stress [51]. In another study, Navai applied increasing tensile and compressive stresses to 302 stainless steel samples. The results indicated that higher tensile stress caused the sample less noble while higher compressive stress caused the sample more noble [52]. However these researches were carried out in neutral or acidic environment, not the high alkaline environment which exists in concrete.

Feng et al. [54] applied several loads to steel bars in simulated pore solution, examining passive behavior under loads and repassivation after load removed. It was found that passive films were more severely damaged under higher loads (5kN and 8kN), while hardly affected by loading time change. They also found that the steel under lower load were able to repassivate after the load removed, but under higher load, which caused plastic deformation, steel could not repassivate by itself. In their research, the impact of compressive stress is not investigated. In addition, depassivation process is not studied. Besides the samples were dried in cold air where the pH is far lower than 9, causing unknown changes in the passive film.

1.3 Motivation

In practice, reinforced concrete structures such as bridges and parking lots slabs always experience variable loads and constant degradation from the aggressive environments, such as deicing salts. Therefore, it is imperative to study the synergic impact of different types of loadings and exposure to chloride ions on the corrosion of steel rebars. Clear understanding of such processes assists improving the resiliency of the structures and helps extending the service life of the constructions by modifying the design codes of structural steel. These modifications will hopefully minimize the maintenance and enhance the durability of the next generation of sustainable infrastructures. In addition, it is necessary to understand the fundamental mechanism of steel passivation and depassivation processes in concrete under stresses, then more reliable and robust service life modeling tools can be made and help engineers to predict the state and performance of rebar in concrete structures. Hence, in order to obtain detailed understanding of the effect of both tensile and compressive stress on passive film and the depassivation process, experiments were performed on steel immersed in concrete simulated pore solution under different types and degrees of loadings. Simulated concrete pore solution was chosen in order to obtain the results in a reasonable time frame required for this project. Several electrochemical measurements including: Cyclic Voltammetry, Electrochemical Impedance Spectroscopy (EIS) and Potentiostatic Linear

Polarization Resistance (PLPR) and Half-cell Potential (HCP) were used. In addition, Mott-Schottky technique was utilized to investigate the semi-conductive behavior of the passive film, formed on the surface of the steel rebars.

CHAPTER TWO

2. EXPERIMENT PREPARATION

2.1 Sample Design and Pre-calculation

In order to study the corrosion behavior of steel under different stresses, a proper sample is necessary. According to ASTM standards Designation: G 39-99 [56], generally there are four typical models of specimen and holder configurations for either beam or sheet, as shown in Figure 2-1, including two-point loaded specimen, three-point loaded specimen, four-point loaded specimen and double beam specimen.

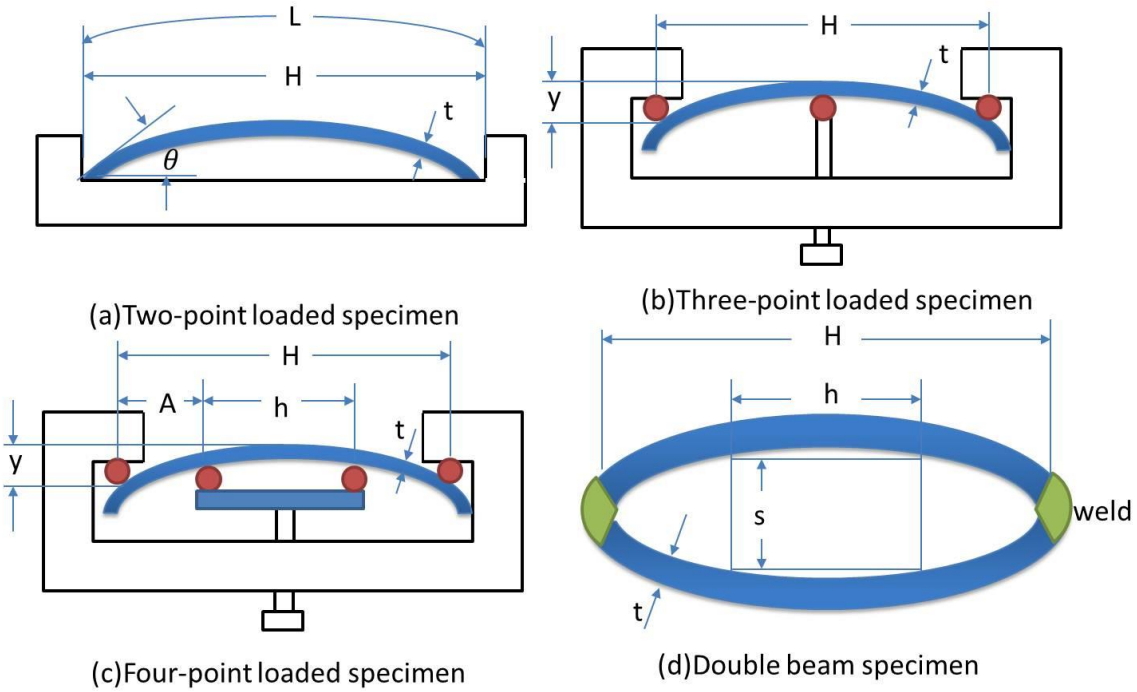

Figure 2-1. Schematic Specimen and Holder Configurations.

These bent-beam specimens are designed for determining the stress-corrosion behavior of metals in a variety of environments and for testing at stress levels below the elastic limit of the alloy. However, each of the models requires a specific and high strength holder or device for anticipated bending range, as shown in Figure 2-2 [56]. Also it would be inconvenient to immerse so many big specimens into pore solution in the lab, which will take too much time and expenditure to accomplish.

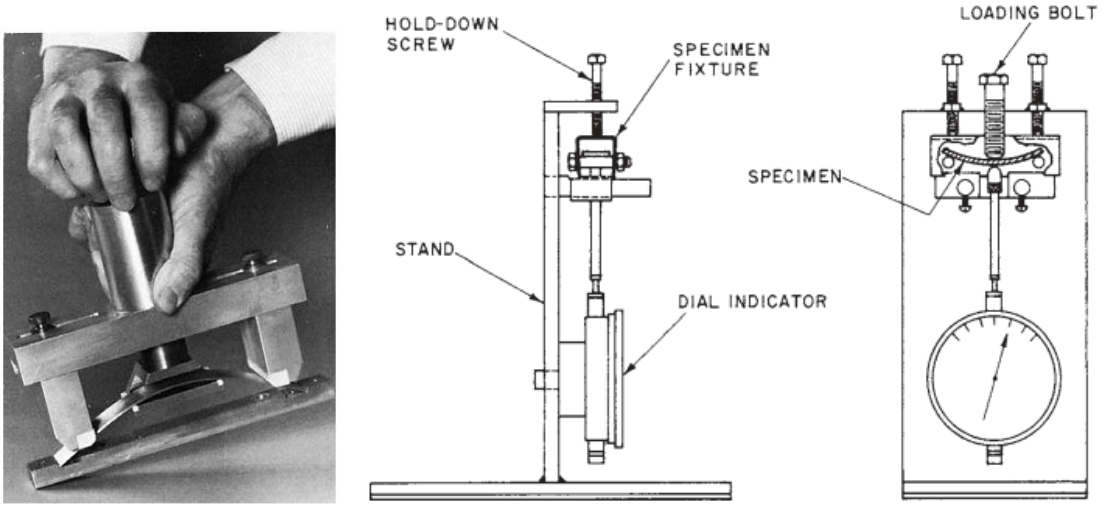

Figure 2-2. Stressing jig and two-point loaded specimen with holder and specimen loading apparatus for three-point loaded beam specimens with integral deflection gage.

Therefore a very handy C-ring model was proposed in this experiment, as shown in Figure 2-3, where the exposed area is the area undertaking most stress and strain. H indicates the displacement of steel ring; by adjusting displacement H from both sides of the sample, different levels of stresses can be achieved.

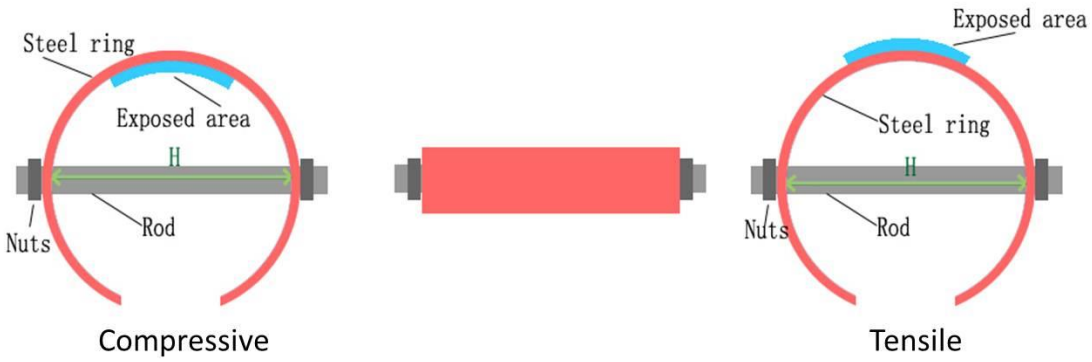

Figure 2-3. Design model of C-ring

Displacements corresponding to different levels of applied stresses were calculated. As seen in Figure 2-4, P stands for the applied stress and H is the displacement of steel ring, meanwhile causing change in both tensile stress (σ_T) and compressive stress (σ_C).

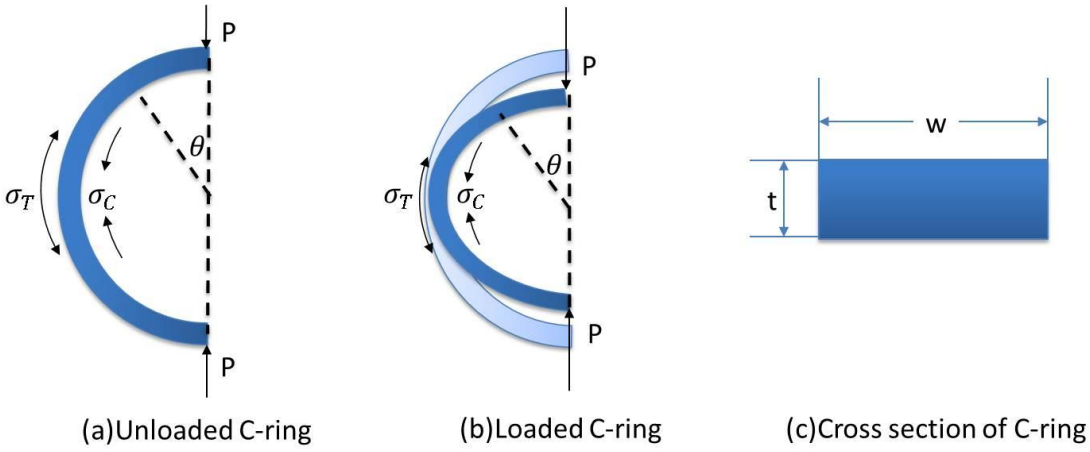

Figure 2-4. Sketch of C-ring

A force F does work when it undergoes a displacement dx which is in the same direction of the force and, the work done U is defined as dU =Fdx. When the total displacement is x, the work can be described as [57]:

$$\boldsymbol{U = \int_0^x F dx} \qquad \text{Equation 2-1}$$

The work done by a couple moment M when it undergoes a rotational displacement dθ along its line of action, (total angle of rotational displacement is θ rad) can be expressed as:

$$\boldsymbol{U = \int_0^\theta M d\theta} \qquad \text{Equation 2-2}$$

In our case, the data can be described as follows:

$$\boldsymbol{M = \frac{PD}{2}} \qquad \text{Equation 2-3}$$

where M is moment, D is diameter, P is pressure.

The moment of inertia I is:

$$\boldsymbol{I = \frac{wt^3}{12}} \qquad \text{Equation 2-4}$$

w is width, t is thickness.

Stress of moment σ_M can be described with moment, thickness and moment of inertia:

$$\boldsymbol{\sigma_M = \frac{Mt}{2I} = \frac{3PD}{wt^3}} \qquad \text{Equation 2-5}$$

$$\boldsymbol{\sigma_P = \frac{P}{A}} \qquad \text{Equation 2-6}$$

Thus compressive and tensile stress can be calculated as follows:

$$\boldsymbol{\sigma_c = \sigma_M + \sigma_P = \frac{Mt}{2I} + \frac{P}{A}}$$ Equation 2-7

$$\boldsymbol{\sigma_t = \sigma_M - \sigma_P = \frac{Mt}{2I} - \frac{P}{A}}$$ Equation 2-8

where σ_c is compressive stress, σ_t is tensile stress. The total work in the loaded sample is:

$$\boldsymbol{U_{total} = U_\mu + U_\nu + U_M}$$ Equation 2-9

where U_μ is the axial energy, U_υ is shear energy and U_M is the moment energy. The axial energy would be:

$$\boldsymbol{U_\mu = \int \frac{P^2 r}{2EA} \, sin^2 \theta \, d\theta}$$ Equation 2-10

E is elastic modulus, A is cross area, P is applied force, r is radius. The shear energy can be shown as:

$$\boldsymbol{U_\nu = \int 3 \frac{P^2 r}{GA} \, cos^2 \theta \, d\theta}$$ Equation 2-11

G is shear modulus of steel

Moment energy is:

$$\boldsymbol{U_M = \int_0^\pi \frac{P^2 r^3}{2EI} \, sin^2 \theta \, d\theta}$$ Equation 2-12

$$\boldsymbol{U_{total} = \int \frac{P^2 r}{2EA} \, sin^2 \theta \, d\theta + \int 3 \frac{P^2 r}{GA} \, cos^2 \theta \, d\theta + \int_0^\pi \frac{P^2 r^3}{2EI} \, sin^2 \theta \, d\theta}$$ Equation 2-13

Since samples are under multiaxial stress, Castigliano's theorem [57] was applied in determining displacement. If the displacement at a point is to be determined, it is equal to the first partial derivative of the strain energy in the body with respect to force acting at the point and in the direction of displacement. Hence the displacement can be determined as followings:

$$\boldsymbol{H = \frac{\partial U total}{\partial P} = \int_0^{\pi} \frac{Pr}{EI}\, sin^2\,\theta\, d\theta + \int_0^{\pi} \frac{6Pr}{GA}\, cos^2\,\theta\, d\theta + \int_0^{\pi} \frac{Pr^3}{EI}\, sin^2\,\theta\, d\theta} \qquad \text{Equation 2-14}$$

$$\boldsymbol{H = \frac{Pr\pi}{2}\left(\frac{1}{EA} + \frac{6}{GA} + \frac{r^2}{EI}\right)} \qquad \text{Equation 2-15}$$

$$\boldsymbol{G = \frac{E}{2(1+\tau)}} \qquad \text{Equation 2-16}$$

where τ is Poisson ratio of low carbon steel. Therefore:

$$\boldsymbol{H = \frac{Pr\pi}{2}\left(\frac{1}{EA} + \frac{6}{GA} + \frac{r^2}{EI}\right)} \qquad \text{Equation 2-17}$$

Compressive stresses and tensile stresses calculated based on the abovementioned method, according to changing displacement, and results are given in Table 2-1.

Table 2-1. Calculation results of different applied stresses. (Yield strength and Ultimate strength of the 1018 low carbon steel are chosen 380MPa and 440MPa, respectively [58])

H/mm	σ_c (MPa)	σ_t (MPa)	P (N)	Percentage of yield strength σ_t / σ_Y
Displacement	Compressive stress	Tensile stress	Force	
0.000	0	0	0	0
1.000	42.303	41.840	9.714	11%
2.000	84.606	83.679	19.429	22%
3.000	126.908	125.519	29.143	33%
4.000	169.211	167.358	38.857	44%
5.000	211.514	209.198	48.572	55%
10.000	423.028	418.395	97.143	110%
15.000	634.542	627.593	145.715	165%

A finite element model was also built based on the materials and loading conditions being used in this experiment to complement the analytical analysis and one of the results is shown in Figure 2-5. Both finite element analysis (FEA) and analytical analysis provide similar results.

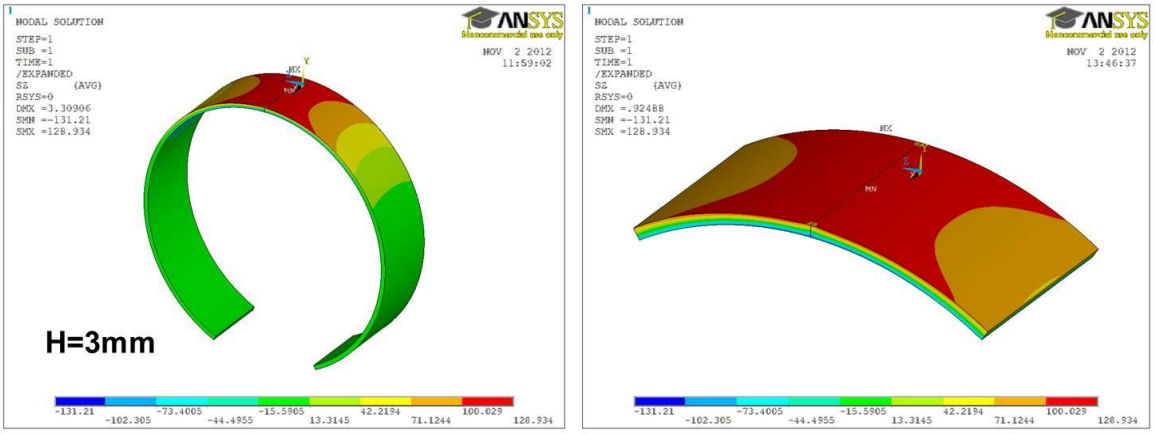

Figure 2-5. FEA analysis of C-ring with increasing displacement

In order to get a distinct trend of the effect of increasing load on corrosion, loading levels from 0, 33%, 55%, 110% to 165% of yield strength, which correspond to the displacement of 0mm, 3mm, 5mm, 10mm and 15mm, respectively, were chosen in this experiment.

2.2 Materials preparation and test procedures

Steel rings were prepared from General purpose 1018 unpolished low-carbon steel pipe, with inner diameter of 3.87 in (98.30mm), outer diameter of 4.00 in (101.6mm) and wall thickness of 0.065 in (1.65mm). High strength plastic rod and nuts were used to control the displacement. To limit the corroded area, to minimize the extraneous effects and, to get a focus observation at the stress concentration, specimens were coated with epoxy resin, except 1.00 in (25.4 mm) as the exposure area, outside and inside for tensile and compressive specimens, respectively (Figure 2-3). Figure 2-5 shows one specimen for each series of tests. To obtain electrical connectivity which is required for the electrochemical tests, a copper wire was connected to each ring before coating.

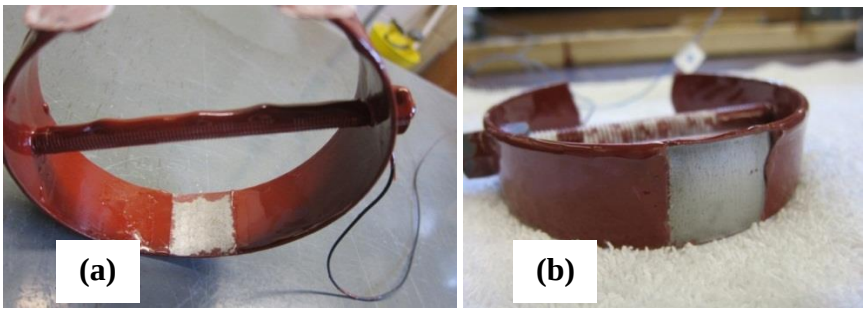

Figure 2-6. One of (a) compressive and (b) tensile specimens.

Simulated concrete pore solution (Type I cement) was prepared with the composition given in Table 2-2. Some studies were conducted on the passivation/depassivation of carbon steel in saturated calcium hydroxide and a concrete simulated pore solution. Poursaee suggested to use simulated concrete pore solution in studying corrosion of steel in concrete other than saturated calcium hydroxide solution, which could change the nature of passive layer [59]. In addition, it was determined by Poursaee and Hansson that the time required for steel to be passivated in concrete simulated pore solution is three days [55].

Table 2-2. Chemical composition of the synthetic pore solution [59].

Compound	Mol/liter
NaOH	0.1
KOH	0.3
$Ca(OH)_2$	0.03
$CaSO_4.H_2O$ (Gypsum)	0.002

Specimens were immersed in pore solution. Since the resolution of carbon dioxide, from atmosphere, in pore solution leads to reduction of the $Ca(OH)_2$ and increase of $CaCO_3$, the pH of solution in micro pores will drop significantly. The passive film becomes metastable with the pH lower than 11.5 and breaks down when pH reduces around 9~10, initiating steel corrosion. Therefore, to avoid carbonation, the container was sealed.

All samples were connected to the VSP-300 potentiostat made by Biologic Science Instruments[2]. For most of the electrochemical tests, a typical three electrode system [36] was used, as illustrated schematically in Figure 2-7. Coated C-ring was the working electrode; saturated calomel electrode and 316 stainless steel sheet were used as a reference electrode and counter electrodes, respectively. To determine the effect of chloride on passive film breakdown, two sets of experiments were conducted: experiment in chloride free and experiment in chloride contaminated pore solutions. For the contaminated solution, specimens were first exposed to the chloride free pore solution for a week and then chloride added to the solution. One week exposure to the chloride free solution guarantied the formation of passive film on all sample with different loading conditions.

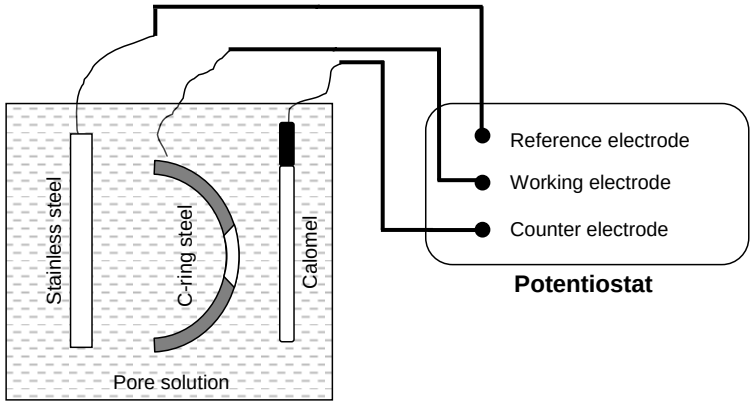

Figure 2-7. Schematic illustration of the setup used in this study

[2] Certain commercial products are identified in this thesis to specify the materials used and procedures employed. In no case does such identification imply endorsement by the author, nor does it indicate that the products are necessarily the best available for the purpose.

2.3 Electrochemical measurements

2.3.1 Half-cell potential

Half-cell potential technique is the most widely applied technique in measuring corrosion of steel reinforcement in concrete. It was introduced by Richard in the 1970s to North America. In 1980 this technique was approved as an ASTM standard as the "Standard Test Method for Half-Cell Potentials of Uncoated Reinforcing Steel in Concrete" [63]. By conducting this test, the electrochemical potential of steel reinforcement in concrete versus a reference electrode is measured. The schematic setup is illustrated in Figure 2-8.

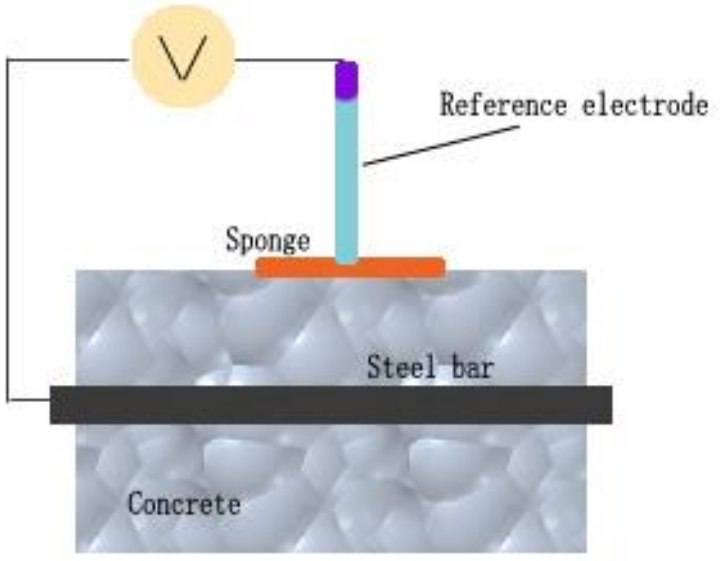

Figure 2-8. Half-cell potential test setup

The half-cell potential of the steel rebar indicates the approximate risk of corrosion. The suggested interpretation of the results according to ASTM can be seen in Table 2-3. However the probability of corrosion should not be taken as the actual corrosion rate, since the test can be disturbed by many factors such as temperature, humidity, etc.

Table 2-3. Probability of corrosion according to half-cell potential reading [63]

Half-cell potential reading versus $Cu/CuSO_4$	Corrosion Activity
More positive than -200mV	90% probability of no corrosion
Between -200 and -350mV	An increase probability of no corrosion
More negative than -350mV	90% probability of no corrosion

2.3.2 Linear Polarization Resistance (LPR)

Figure 2-9 shows a schematic plot of the relationship between potential and current in the region of the open circuit potential. The curve plots the applied potential versus measured current or vice versa. As shown in Figure 2-9, there is an approximately linear region around the open circuit potential. The LPR measurements are performed by applying a potential in the range of ±10mV about the E_{corr}, either as a constant pulse (potentiostatic) or a potential sweep (potentiodynamic) and measuring the current response. Polarization resistance (R_p) is the resistance of the specimen to oxidation while an external potential is applied and the corrosion rate which is inversely related to the R_p can be calculated from it.

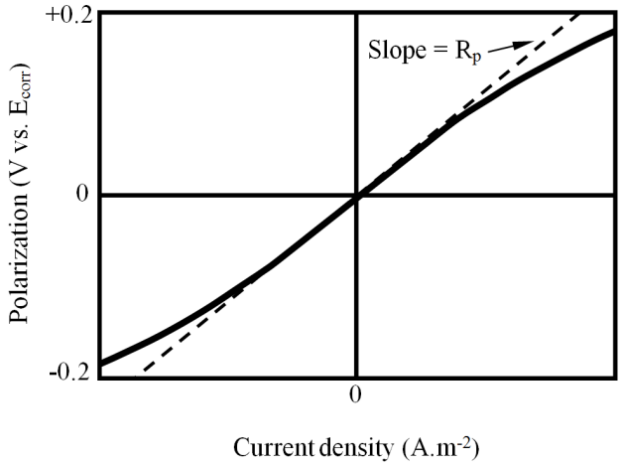

Figure 2-9. Schematic illustration of the linear polarization curve.

R_p is determined by calculating the slope of this linear region [64]:

$$\boldsymbol{R_p = \frac{\Delta E}{\Delta I}} \qquad \text{Equation 2-18}$$

where, ΔE = change in potential and ΔI = change in current. The Stern-Geary equation relates corrosion current to R_p [64]:

$$\boldsymbol{I_{corr} = \frac{B}{Rp}} \qquad \text{Equation 2-19}$$

$$\boldsymbol{B = \frac{\beta_a \beta_c}{2.3 i_{corr}(\beta_a + \beta_c)}} \qquad \text{Equation 2-20}$$

The corrosion current density, i_{corr}, can be calculated by dividing the corrosion current (I_{corr}) by the surface area of the polarized area (A):

$$\boldsymbol{i_{corr} = \frac{B}{R_p A}}$$ Equation 2-21

B is Stern-Geary constant and β_a and β_c are anodic and cathodic Tafel constants, respectively. The value of B should be determined, empirically. However, for most cases, it can be assumed to be 0.026V for active and 0.052V for passive corrosion of steel in concrete [65] [66].

In the potentiostatic LPR test a constant potential is applied for a certain period of time, during which the current can reach a stable state and ΔI, in Figure 2-10, can be determined. The polarization resistance, R_p, [67] and corrosion current I_{corr} can be calculated from ΔE and ΔI:

$$\boldsymbol{R_p = \frac{\Delta E}{\Delta I}}$$ Equation 2-22

$$\boldsymbol{I_{corr} = \frac{B}{Rp}}$$ Equation 2-23

Hence the corrosion current density i_{corr} can be calculated from deviding the corrosion current I_{corr} by the surface area of the polarized area A:

$$\boldsymbol{i_{corr} = \frac{B}{R_p A}}$$ Equation 2-24

In this study, ±10 mV, versus the open circuit potential for 60 seconds was used for the test.

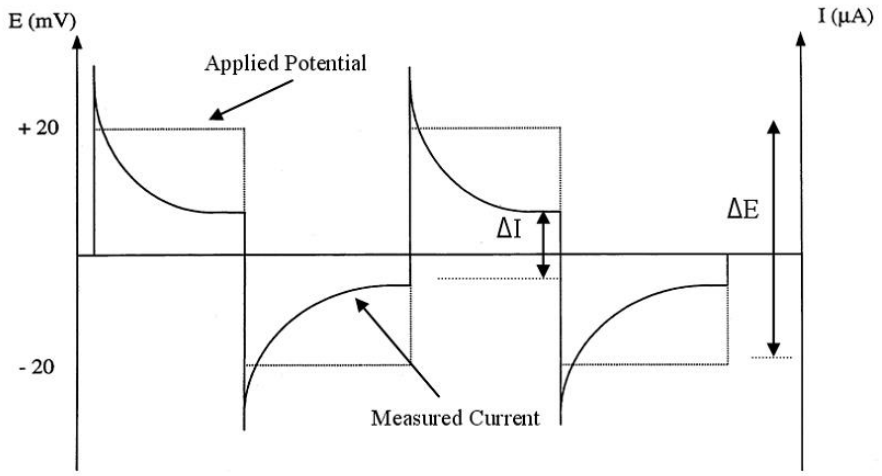

Figure 2-10. Concrete resistance

2.3.3 Electrochemical Impedance Spectroscopy (EIS)

The EIS studies the system response to the application of a small amplitude alternating potential or current signal at different frequencies. The popularity of the EIS methods for reinforced concrete has increased remarkably in recent years, because analysis of the system response provides information about the double-layer capacitance, interface, structure, reactions which are taking place, corrosion rate and electrolyte (environment) resistance [49,68,69]. An electrochemical process can be considered as an electrical circuit with basic elements such as resistors, capacitors and inductors. Therefore, in interpreting the response to an AC current, the AC circuit theory can be used successfully to demonstrate of a corrosion process and also it may be used to understand the behavior of the corrosion process and prediction of the corrosion rates.

In direct current, the Ohm's law is as following:

$$\boldsymbol{V = IR}$$ Equation 2-25

(V= Potential, I = Direct current, R= Actual resistor)

In the AC condition, Ohm's law becomes:

$$\boldsymbol{V = IZ}$$ Equation 2-26

(V= Potential, I = Alternative current, Z= Impedance)

Direct current can be viewed as alternating current at zero frequency. In this case, the resistance is composed of only one or more actual resistors. When the frequency is not zero, all circuit elements that can affect the flow of current, e.g., resistors, capacitors, and inductors cause the resistance. The created resistance by capacitors and inductors depends on frequency while that created by a resistor is not dependant on frequency [70]. A sinusoidal current or voltage can be represented as a rotating vector as shown in Figure 2-11. In this Figure, the x component shows the observed current so it becomes the real component of the rotating vector while the y component is a contribution that is not observed; therefore it is named the imaginary component of the rotating vector.

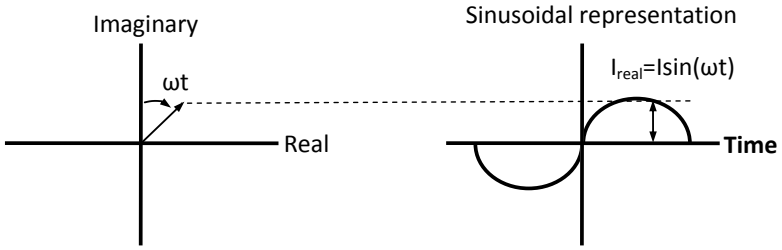

Figure 2-11. Relationship between sinusoidal AC current and rotating vector representation

The mathematical descriptions of the two components are as followings:

$$\text{Real current} = I_x = |I| \cos(\omega t) \qquad \text{Equation 2-27}$$

$$\text{Imaginary current} = I_y = |I| \sin(\omega t) \qquad \text{Equation 2-28}$$

where t = time and ω = frequency in radians per second = 2πf (f = frequency in Hertz)

To separate the real (x) and imaginary (y) components, the magnitude of the imaginary part should be multiplied by $j = \sqrt{-1}$ [3] and then the real and imaginary values can be reported separately. The equations for AC impedance become:

$$E_{total} = E_{real} + E_{imaginary} = E' + jE'' \qquad \text{Equation 2-29}$$

$$I_{total} = I_{real} + I_{imaginary} = I' + jI'' \qquad \text{Equation 2-30}$$

$$\boldsymbol{Z_{total} = Z' + Z'' = \frac{E' + jE''}{I' + jI''}} \qquad \text{Equation 2-31}$$

Absolute amplitude of the impedance (that is the length of the vector) and the phase angle are defined by [71]:

$$|\mathbf{Z}| = \sqrt{\mathbf{Z'}^{2} + \mathbf{Z''^{2}}} \qquad \text{Equation 2-32}$$

[3] Mathematicians use i to stand for, but electrochemists use j to avoid confusion with i, the symbol for current.

$$\tan\theta = \frac{Z''}{Z'} \qquad \text{Equation 2-33}$$

The goal of AC impedance is to measure the impedance Z as Z' and Z", and then model the response by using an equivalent simple circuit [70].

2.3.3.1 Data presentation

There are different ways to illustrate the response of an electrochemical system to an applied AC potential or current. The most common plots are the Nyquist plot and Bode plots. If, at each excitation frequency, the real part is plotted on the x-axis and the imaginary part is plotted on the y-axis of a chart, a "Nyquist plot" is formed. A simple corroding system can be assumed as: solution resistance, in series with a combination of a resistor and a capacitor, which represent the polarization resistance and double layer capacitance, respectively. This is simple representation is called Randles cell and is shown in Figure 2-12.

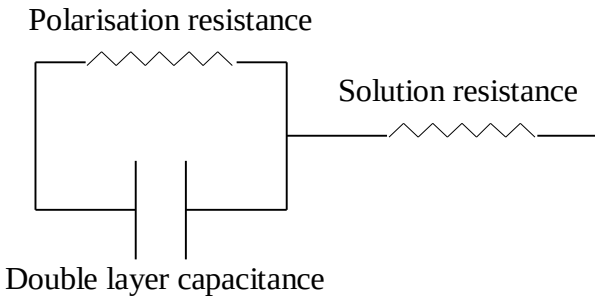

Figure 2-12. Equivalent circuit for a simple electrochemical system.

Figure 2-13 schematically illustrates the Nyquist plot for a simple electrochemical system corresponding to the analogue circuit in Figure 2-12. It should be noted that each point on the Nyquist plot is the impedance at one frequency. On the Nyquist plot, the impedance can be represented as a vector of length |Z| and the angle between this vector and the x-axis, is the phase angle "θ" [71,72]. At high frequencies, at the leftmost end of the semicircle, where the semicircle touches the x-axis, the impedance of the Randles cell is entirely produced by the ohmic resistance, R_Ω. The frequency reaches its low limit at the rightmost end of the semicircle. At this frequency, the Randles cell also approximates a pure resistance, but now the value is $(R_\Omega + R_p)$ [71].

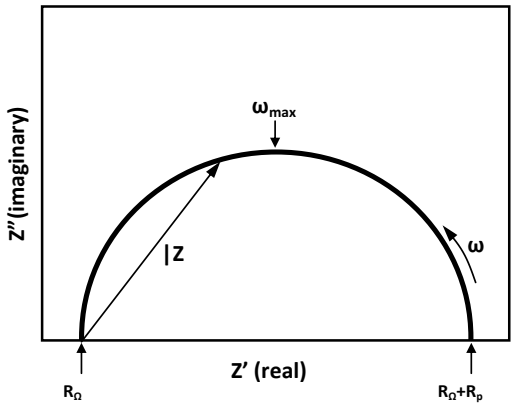

Figure 2-13. Nyquist plot for a simple electrochemical system

The Nyquist plot has some limitations [71]:

(i) The frequency is not clearly shown on the plot and it is not possible to determine, for a specific point, the frequency used to the record that point;

(ii) The ohmic and polarization resistances can be directly determined from the plot but the electrode capacitance can be only calculated if the frequency information is known, using eq. 2-34:

$$\mathbf{C} = \frac{\mathbf{1}}{\boldsymbol{\omega}_{\mathbf{max}}\mathbf{+R_p}} \qquad \text{Equation 2-34}$$

(iii) If there are high and low impedance components in the circuit, the larger impedance controls plot scaling and distinguishing the low impedance semicircle would probably be impossible.

A Bode plot is another popular presentation method for the impedance data. In the Bode plot, the data are plotted with log of frequency on the abscissa and both the log of absolute value of the impedance (|Z|) and phase-shift (θ) on the ordinate [72]. Figure 2-14 schematically shows a Bode Plot for the same system shown in Figure 2-12. Since the frequency appears in as one of the axes in the Bode plot, it is easy to understand the dependence of impedance to the frequency from the plot. The log |Z| vs. log ω curve can be used to determine the values of R_p and R_Ω. At very high and very low frequencies, |Z| becomes independent of frequency. At the highest frequencies the ohmic resistance controls the impedance and log (R_Ω) can be read from the high frequency horizontal level. On the other hand, at the lowest frequencies, polarization resistance contributes, and log ($R_p + R_\Omega$) can be read from the low frequency horizontal portion.

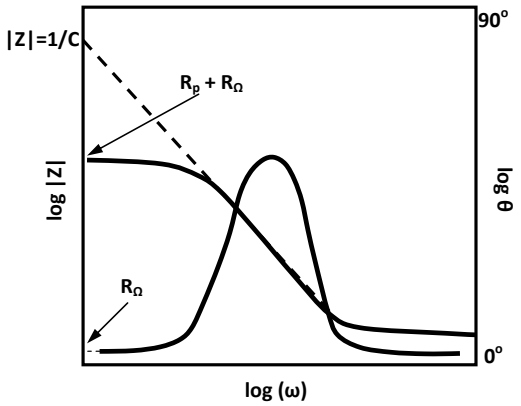

Figure 2-14. Bode plot for the same system shown in figure 2-11.

The Bode format is advantageous when data scatter prevents satisfactory fitting of the Nyquist semicircle. In general, the Bode plot provides a more understandable description of the frequency-dependent behavior of electrochemical system than does the Nyquist plot, which frequency values are not clear [71].

Since one of the objectives of this research was to investigate the semi conductivity of passive film in pore solution, the Staircase Potentio-Electrochemical Impedance (SPEIS) technique was applied. SPEIS consists of a staircase potential sweep. In SPEIS test different potential steps can be applied in the same experiment and, for each potential step, an electrochemical impedance spectroscopy measurement is done. With the results electrochemical reaction kinetics of tested specimen along steady-state curves can be studied. Using the SPEIS, the Mott Schottky plots can be obtained for each specimen which provides information on the semi conductive behaviors of passive film.

Semi-conductive parameters, i.e. donor density, based on the Mott-Schottky relationship can then be determined. In this study, 1 kHz was chosen to analyze the

results from Mott-Schottky plots, and the chosen dielectric constant was 12 for the passive later [46], the surface area is given in pre-calculation part as 6.4516cm^2.

2.3.4 Cyclic voltammetry

Cyclic voltammetry (CV) is a popular electrochemical measurement which was first introduced by Kemula [78], and widely applied later on solid electrodes, with the purpose of investigating the anodic oxidations [79].

CV is one type of potentiodynamic electrochemical measurement in which a cyclic waveform potential is applied to the working electrode, the potential is in a triangle shape and changes linearly with time, as given in figure 2-15. The slope (V/s) is the scan rate; one cycle is completed after it scans from starting potential to terminating potential. The results of CV measurement can be plotted in a Current vs. Potential curve that is often used to estimate the reversibility of electrode reaction and predict formation of intermediate product or new phase, and so on [22].

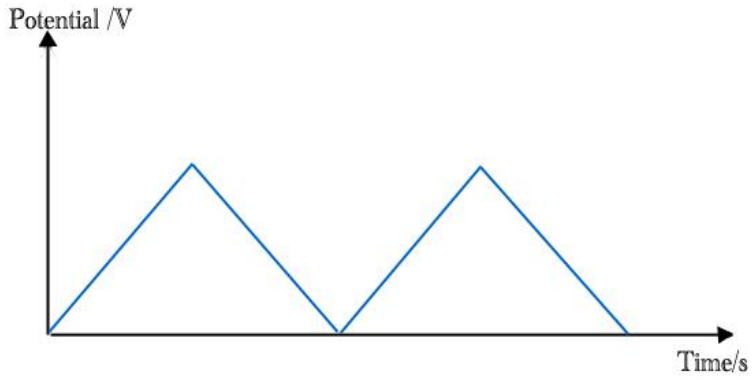

Figure 2-15. Cyclic voltammetry potential waveform

In this research the working electrode potential continuously cycled from -1.4V to +0.4 V with scan rate of 50mV/s, repeating 10 times.

2.4 Experiment schedule

For the half cell potential, corrosion current density and the Mott Schottky analysis, all samples (0 load, 3mm, 5mm, 10mm and 15mm under both tensile and compressive loads) were immersed in simulated pore solution and the measurement was performed twice a day for ten days. After the chloride free test, the corrosion behavior of samples in chloride contaminated pore solution was examined, where 5 wt% NaCl was added after first test in chloride free solution. At the end of 10^{th} day immersion, another 5 wt% NaCl was added and the electrochemical performance of steel in pore solution with chloride concentration at 10 wt% was tested once a day for 10 days.

For the cyclic voltammetry test, 0 load and 10mm (tensile stressed) were measured. Samples were immersed for 24 hrs in chloride free pore solution, and then first CV test was performed. Five days later the second CV test was carried out and then 3 wt% NaCl was added into the pore solution 24 hours and 5 days after adding the chlorides, CV test was performed again on the specimens.

CHAPTER THREE

3. RESULTS AND DISCUSSIONS

All measurements were performed on two identical specimens of each loading conditions. Since the results of the tests on two specimens were very close and very similar, just the results of one of the specimens for each loading conditions is presented in this chapter.

3.1 Experiments in chloride free pore solution

3.1.1 Corrosion potential

Figures 3-1a and 3-1b show the corrosion (half-cell) potential values measured versus $Cu/CuSO_4$ reference electrode for the samples immersed in chloride free pore solution under tensile and compressive stresses, respectively. It can be seen that with immersion time extending, the potential of samples rose to more positive level. Besides, under tension the samples reached more negative potential when stress increased, while for samples under compressive stress, the trend came in an opposite way that higher stresses led to more positive potential. With respect to the specimen with no load, specimens under tensile loads exhibit more positive potentials compare to those under compressive stress.

The difference between tensile and compressive samples is possibly caused by the passive film formed on the exposed area. The specimens under tensile stress initially corrode faster than the specimens under compressive stress. Since passivation is oxidation on the surface, the more corrosion on the surface of the specimens under tensile stress leads to better initial passivation in this condition. Therefore, more positive potentials for specimens under tensile stress, which corresponds to passivation, can be obtained compared with that for the specimens under compressive stress. More positive potential for the specimens under tensile loading conditions indicates more protective passive film on those specimens.

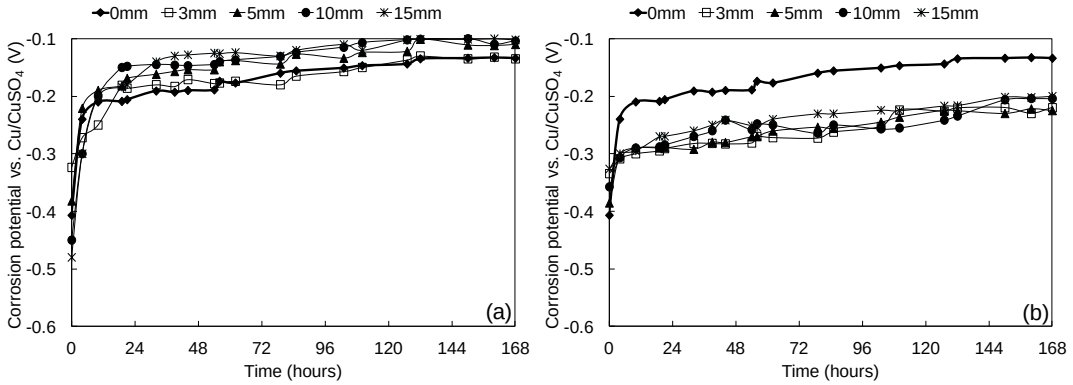

Figure 3-1. Half-cell potential of specimens in chloride free pore solution
(a) under tension (b) under compression

3.1.2 Corrosion current density

Figures 3-2a and 3-2b show the corrosion current densities of the specimens, measured by potentiostatic LPR. In Figure 3-2 it is found that with immersion time went on, the current densities of all specimens decreases to below 10^{-3} A/m^{-2}, which is

considered as the passive current density. The required time for passivation is about 24 hours which is in agreement with what have been observed from corrosion potential measurements. In addition, the current densities on the specimens under tensile loadings exhibit lower values compared with those under compressive loadings. While this difference is very small, but it show more rapid passivation time and slightly more protective passive layer in specimens under tensile loading conditions. This is in agreement with the corrosion potential measurements and therefore validates the hypothesis explained in section 3.1.1 for such behavior.

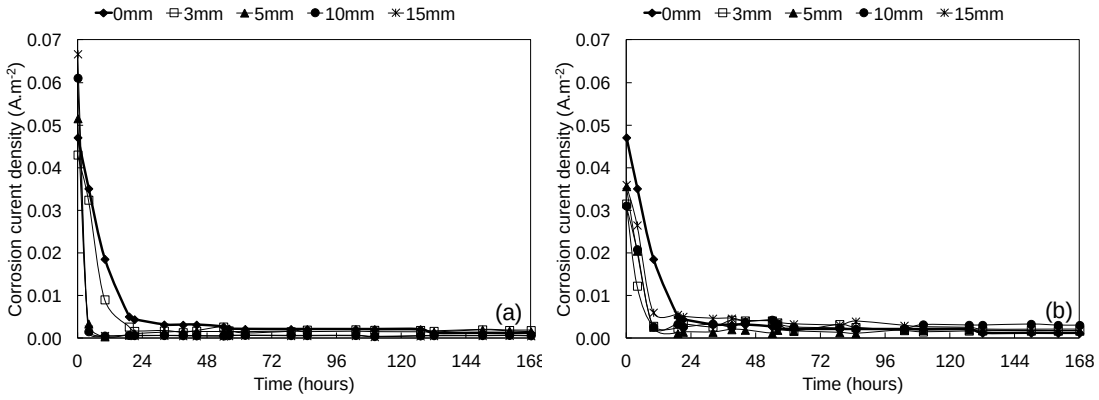

Figure 3-2. Corrosion current density of specimens in chloride free pore solution (a) under tension (b) under compression

3.1.3 Mott-Schottky

The charge distribution at the semiconductor and electrolyte interface was calculated by measuring the capacitance of the space-charge layer (C_{SC}) as a function of the electrode potential. The values of $(1/C_{sc})^2$ of the specimens determined at 1000 Hz. The corresponding Mott-Schottky plot (C_{sc}^{-2} versus potential) was determined at different

times up to 168 hours. Mott-Schottky plots for specimens under tensile and compressive stresses, after 96 hours of exposure to pore solution is shown in Figure 3-3. It should be mentioned that the scale of Y-axis in Figures 3-3a and 3-3b are different. As can be seen, the slope of the plot is positive which illustrates the properties of n-type semiconductors. The slopes of the Mott-Schottky plots changed with the magnitude of the applied stress. The slopes of the Mott-Schottky plots of the specimens under tensile stress with larger loads are smaller than those acquired in smaller loadings conditions, while specimens under compressive loading, exhibit opposite behavior.

In addition, the slopes of the plots for specimens under compressive stresses are much larger than those for the specimens under tensile stresses. As discussed before, the larger the Mott-Schottky plot slope, the smaller the donor density, the thicker the space-charger layer and consequently, the thicker the passive film layer. This observation is in agreement with what have been found from the measurement of the corrosion potentials and corrosion current densities.

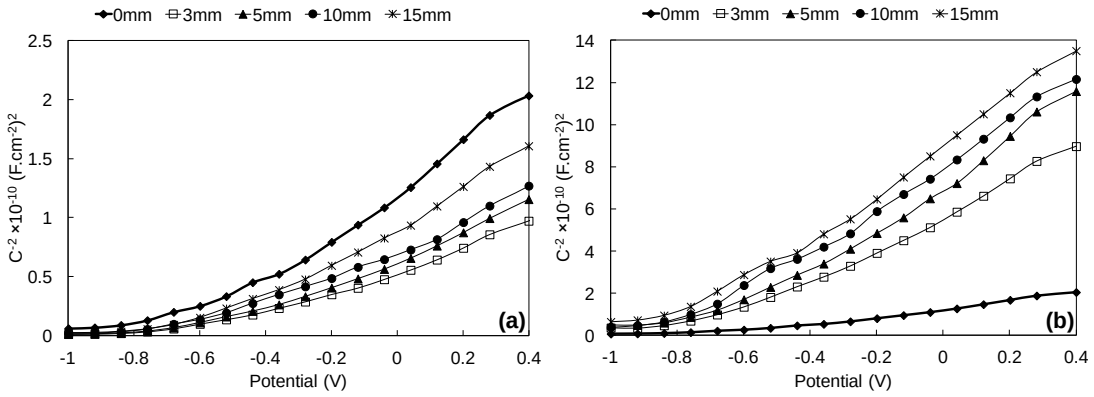

Figure 3-3. Mott-Schottky plots of specimens in chloride free pore solution (a) under tension (b) under compression

3.1.4 Donor density

Figures 3-4a and 3-4b show the donor density versus time obtained from the Mott-Schottky plots for specimens under tensile and compressive loading conditions, respectively. Up to 24 hours after exposure, the donor density increases for all specimens. It means that the density of current carrying components in the semiconductive passive film is increased up to 24 hours and then it starts to decrease which indicates less conductivity and thicker semiconductive film. This corresponds to the time of passivation, determined by corrosion potential and corrosion current measurements.

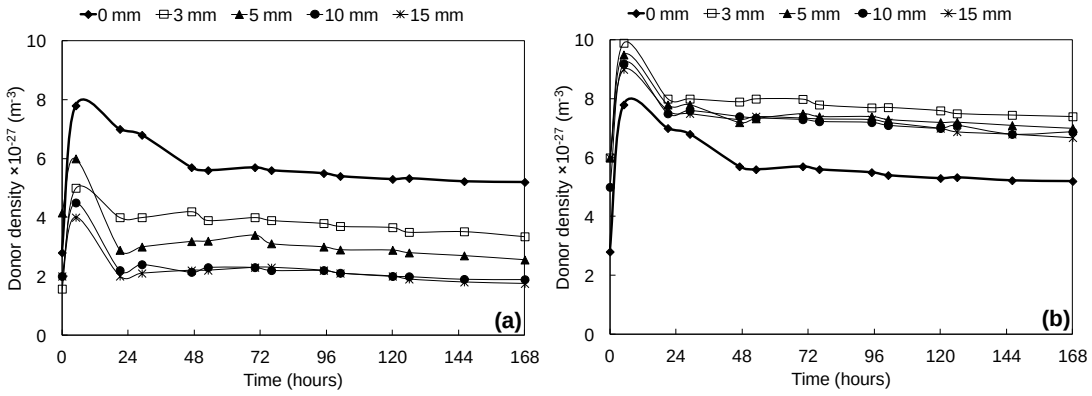

Figure 3-4. Donor density of specimens in chloride free pore solution
(a) under tension (b) under compression

The slopes of the graphs in both cases are generally negative, indicating growth of the passive film. As can be seen, the donor densities of the specimens under tensile loading condition are lower than that for the specimen under no load, while specimens under compression show opposite behavior. This again confirms the hypothesis that

under tensile conditions, the passive film is more protective compare to that under compressive loading conditions.

3.2 Experiments in chloride contaminated pore solution

To study the effect of chloride on corrosion behavior, 5% wt NaCl was added after 24 hours and another 5% NaCl added after 240 hours of immersion in pore solution.

3.2.1 Half-cell potential

Unlike the samples in chloride free pore solution, specimens in chloride contaminated solution showed different performance during the test. Figures 3-5a and 3-5b show the corrosion potential values measured versus $Cu/CuSO_4$ for the specimens under tensile and compressive stresses, respectively. It can be seen that during the immersion period, the potential of both groups (tensile and compressive) exhibit similar trend. that from -0.26V at the beginning sharply decreased to about -0.55V after about 48 hours and then stayed almost steadily at this level before increasing the NaCl concentration. With NaCl addition, a small peak can be found around 240 hours in all the curves, where the potentials were in a slowly decreasing state. However the change is not significant due to severe corrosion before that point. Specimens under tensile stress show more negative potentials than specimen with no load. On the other hand, specimens under compressive stresses exhibit more positive potential than the control specimen (no load). This observation indicates that the tensile loading can increase the

susceptibility of steel against corrosion due to chloride attack while compressive stress decreases it.

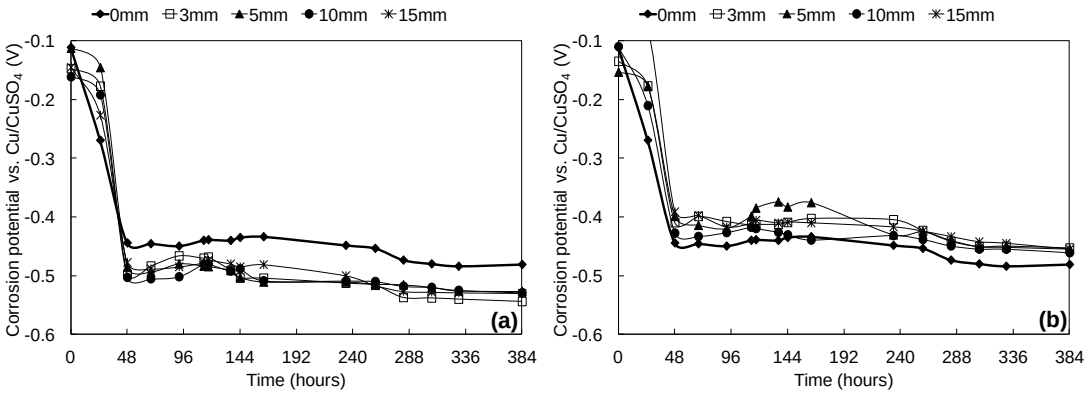

Figure 3-5. Corrosion potential of specimens in chloride contaminated solution (a) under tension (b) under compression

3.2.2 Corrosion current density

As seen in Figure 3-6, short time after adding 5% chloride to the solution, corrosion current density increased to active corrosion. When chloride concentration reached 10%wt at 240 hours, corrosion current density rises for both groups of specimens. In Figure 3-6a, specimens under tensile exhibit higher corrosion current compare to the control specimen (no load). However, specimens under compressive stress perform oppositely and generally corrode at lower rates than the control specimen. This behavior shows the negative impact of the tensile stress on the corrosion activity of the steel when exposed to the chlorides. While there is no distinguished trend among compressive stresses, generally, higher tensile stress leads to more active corrosion.

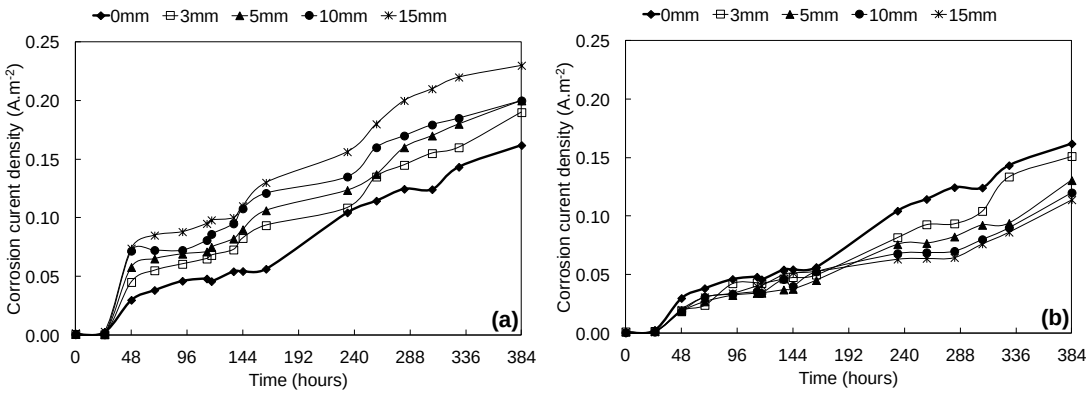

Figure 3-6. Corrosion current density of specimens in chloride contaminated solution (a) under tension (b) under compression

3.2.3 Donor density

Figures 3-7a and 3-7b show the donor density versus time obtained from the Mott-Schottky analysis for the specimens under tensile and compressive loadings, respectively. As can be seen, the donor densities in both groups increased, exhibiting more conductivity in the semiconductive surface layer on the steel. The presence of chlorides significantly increases the donor density and consequently causes active corrosion.

The slopes of the graphs in both cases are positive, indicating more corrosion activity on the surface of the steel. As can be seen, the donor densities of the specimens under tensile loading conditions are higher than that for the control specimen (no load), while there is no trend among specimens under compressive stress. This again confirms the hypothesis that under tensile conditions, the specimens undergo more active corrosion.

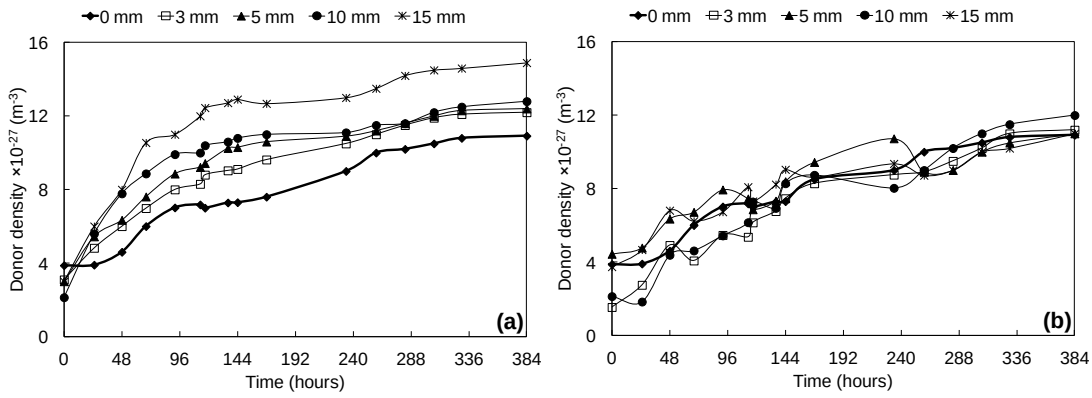

Figure 3-7. Donor density of specimens in chloride contaminated solution (a) under tension (b) under compression

3.3 Cyclic voltammetry

During the cyclic voltammetry test, two specimens were used: 0mm (control-no load) and 10mm, tensile. After 5 days of immersion in simulated pore solution, 3% wt NaCl was added. Specimens were kept in this solution for 5 days. Measurements were performed 24 and 120 hours after exposure to chloride free pore solution and 10 minutes and 120 hours after exposure to the chloride contaminated pore solution.

As seen in Figure 3-8, when no chloride exists in the pore solution there are two anodic peaks (a1 and a2) and one cathodic peak (c1). There is also another peak, named H, which corresponds to the hydrogen evolution. Peak a1 attributed to the formation of a film of $Fe(OH)_2$ and/or FeO. Peak a2 corresponds to the transformation of Fe^{2+} to Fe^{3+}. Peak c1 is considered to be the reduction reactions corresponding to the anodic reactions at peak a2 [80-82]. There is no considerable difference between control specimen and the specimen under tensile stress (10mm). After 120 hour exposure, specimen under tensile stress shows higher current density value for peaks a1 and a2 compare to the control

specimen. This is an indication of more oxidation reactions due to passivation process when specimen is under tensile stress. 10 minutes after addition of the chlorides to the solution, both specimens show higher current density values in their *a* peaks.

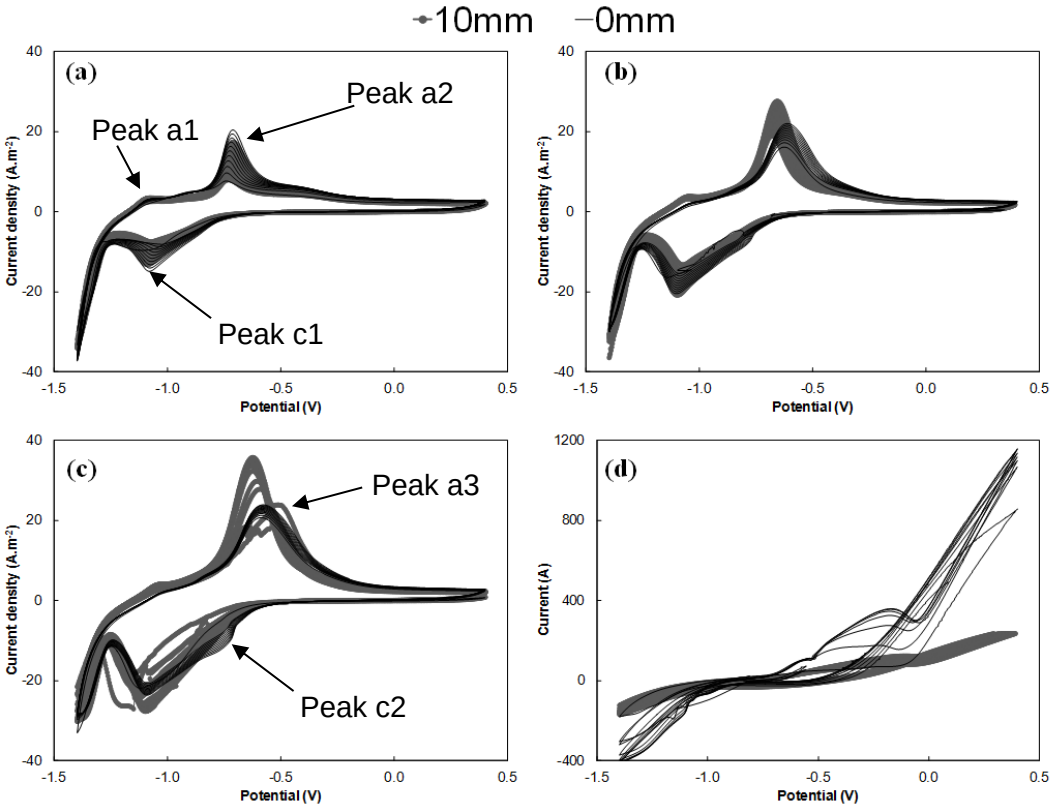

Figure 3-8. Voltammogram for control specimen (0mm) and specimen under tensile stress (10mm): (a) 24 hours in chloride free solution, (b) 120 hours in chloride free solution, (c) 10 minutes in 3% chloride contaminated solution and (d) 120 hours in 3% chloride contaminated solution

However, in specimen under tensile stress, two peaks, a3 and c2, appear on the anodic and cathodic portions of the voltammogram, respectively. Peak a3 can be attributed to an oxidation within the compact passive layer, involving formation of the Fe_2O_3, Fe_3O_4, or FeOOH. And peak c2 is considered to be the result of the reduction

reactions for peak a3 [80,81]. 120 hours after exposure to the chloride contaminated pore solution, extensive depassivation is observed and the voltammogram being extremely disordered with very large current flowing throughout. This is more significant in the normally plateau passive region.

3.4 Impedance spectroscopy

For the impedance spectroscopy measurements, three specimens were used: 0mm (control-no load) 10mm under tensile and compressive stresses. After 5 days of immersion in simulated pore solution, 3% wt NaCl was added. Specimens were kept in this solution for 5 days. Measurements were performed 24 hours after exposure to chloride free pore solution and 24 hours after exposure to the chloride contaminated pore solution and the results are shown in Figure 3-9a and 3-9b. As can be seen in Figure 3-9a, specimen under tensile stress passivates before two other specimens in chloride free pore solution. However, by adding chlorides to the solution, specimen under tensile shows more rapid corrosion compare to the other specimens. These results are in agreement with the results from the other electrochemical experiments.

In addition, visual examination of the corrosion specimens under tensile and compressive stresses confirms the electrochemical measurements as shown in Figure 3-10. As can be seen, more corrosion is observed on the surface of the specimen under tensile compared with that under compressive stress after 5 days exposure to chloride contaminated pore solution.

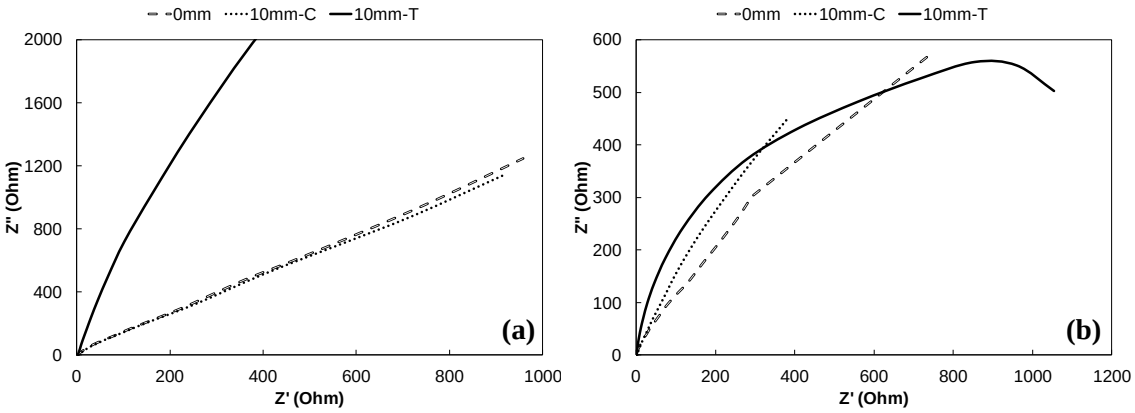

Figure 3-9. Nyquist plots for control specimen (0mm) and specimens under tensile and compressive stresses (10mm); (a) 24 hours in chloride free solution and (b) 24 hours in chloride contaminated solution

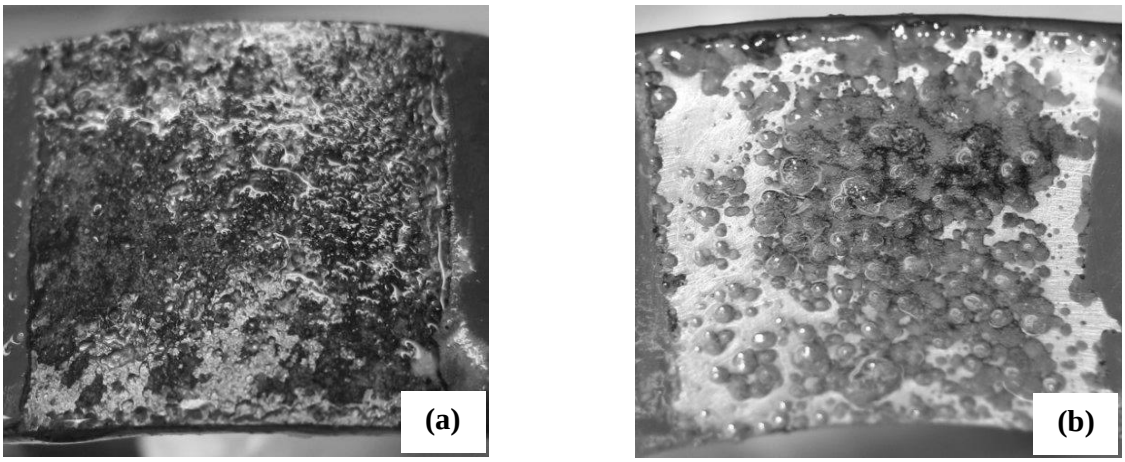

Figure 3-10. Photograph of the surface of one of the specimens after 5 days of exposure to the chloride contaminated solution;
(a) under tensile stress and (b) under compressive stress

CHAPTER FOUR

4. CONCLUSION

Results from different electrochemical tests show that specimens under different loading conditions behave differently during passivation and depassivation processes in concrete simulate pore solution. In chloride free pore solution, the corrosion current density is less for the specimens under tensile stresses than for those under the compressive stresses. This means that the passivation for the concave side (compressive) occurs more rapidly than for the convex side (tensile). The electrode potential of the specimens under tensile stresses becomes more noble with increasing tensile stress. On the contrary, increase of the compressive stress leads to minor decrease in the nobility of the potential. This can be hypothesizes as specimens under tensile stress oxidize more with higher rate.

However, when pore solution is contaminated with the chlorides, opposite behavior is observed. Specimens under tensile stress corrode faster that those under compressive stresses and no stress. On the other hand, specimens under compressive stress show better performance than those under no loading condition, when exposed to chlorides. In spite of having more protective passive later under tensile stresses, this layer cannot protect the steel effectively when it is exposed to chlorides. The impact of stress is far more significant than the effect of passive layer in protecting the steel against corrosion. One reason could be different nanostructure of the passive layer, formed under tensile compare to that formed under compressive stresses. More porous passive

layer with nano-cracks on the steel under tensile could cause rapid dissolution of this layer against chlorides. While there is no distinguished trend among compressive stresses, generally, higher tensile stress leads to more active corrosion.

Regardless of the type and magnitude of the applied load, the passive film on rebar in concrete simulate pore solution is a highly disordered n-type semiconductor. In the presence of chlorides, the slope of the Mott-Schottky plots decreases and donor density increases, which causes decreased corrosion resistance and a thinner passive film on rebar. Consequently, the passive film tends to be more susceptible to breakage.

CHAPTER FIVE

5. RECOMMENDATIONS

- It is clear that steel behaves differently under different loading conditions. However, more study is required to clarify the mechanism of corrosion under different loading conditions. In addition, the micro and nano-structure of the passive layer needs to be studied in different loadings.
- The critical chloride concentration (chloride threshold value) needs to be determined for each level of both tensile and compressive loadings.
- Corrosion products on the surface of steel under different loadings need to be analyzed.
- This study was focused on the static loading, while steel reinforced structures are often subjected to dynamic loadings as well. Therefore, it is suggested that the impact of dynamic loading on passivation and depassivation processes due to corrosion also be investigated.
- This study was performed in concrete simulated pore solution in small scale. For the results to be more representative, it is recommended that the corrosion of the steel reinforced concrete specimens under different loadings be studied as well.
- Carbonation is the other cause of corrosion of steel bars in concrete. Since the mechanism of corrosion due to carbonation is different from that during chloride attack, it is important to study the impact of different loading conditions on the passivation and depassivation of steel during carbonation as well.

APPENDICES

Appendix A. Specifications of 1018 low carbon steel pipe

OD (mm)	ID (mm)	radius (mm)	Width (mm)	Thickness (mm)	E (MPa)	G (MPa)	Yield strength (MPa)
101.600	98.298	49.97	25.400	1.651	200,000.000	75,000.000	380.000

Appendix B. Calculation of stress according to displacements

Displacement H (mm)	Pressure P (N)	Compressive stress σ_c (MPa)	Tensile stress σ_t (MPa)	Percentage of yield strength
1.000	9.714	42.303	41.840	11%
2.000	19.429	84.606	83.679	22%
3.000	29.143	126.908	125.519	33%
4.000	38.857	169.211	167.358	44%
5.000	48.572	211.514	209.198	55%
6.000	58.286	253.817	251.037	66%
7.000	68.000	296.120	292.877	77%
8.000	77.715	338.422	334.716	88%
9.000	87.429	380.725	376.556	99%
10.000	97.143	423.028	418.395	110%
11.000	106.858	465.331	460.235	121%
12.000	116.572	507.634	502.074	132%
13.000	126.286	549.936	543.914	143%
14.000	136.001	592.239	585.753	154%
15.000	145.715	634.542	627.593	165%

REFERENCES

[1] G.H. Koch, N. G. Thompson, Y. P. Virmani, and J . H. Payer, "Corrosion Costs and Preventive Strategies in the United States.," Federal Highway Administration (FHWA), Office of Infrastructure Research and Development, Washington DC, 2001.

[2] Yunovich, M., N.G. Thompson, T. Balvanyos, and L. Lave, "Corrosion Costs and Preventive Strategies in the United States, Appendix D: Highway Bridges.," Federal Highway Administration (FHWA), Office of Infrastructure Research and Development, Washington DC, 2001.

[3] Tavakkolizadeh, Mohammadreza, and Hamid Saadatmanesh., " "Galvanic corrosion of carbon and steel in aggressive environments."," Journal of Composites for Construction, vol. 5.3, pp. 200-210., 2001.

[4] A. Bentur, Steel corrosion in concrete: fundamentals and civil engineering practice., Taylor & Francis, 1998.

[5] Frangopol, Dan M., Kai-Yung Lin, and Allen C. Estes., " "Reliability of reinforced concrete girders under corrosion attack."," Journal of Structural Engineering , vol. 123, pp. 286-297., 1997.

[6] Sidney Mindess, J.Francis Young, Concrete, Prentice-Hall, 1981.

[7] K.Andersson, B.Allard., "Chemical composition of cement pore solutions.," vol. 19, 1989.

[8] "ACI 318-05 Building Code for Structural Concrete".

[9] Kimiro Meguro, Motohiko Hakuno., "Fracture analysis of concrete structures by the modified distinct element method.".

[10] J. G. MacGregor, REINFORCED CONCRETE: MECHANICS AND DESIGN.

[11] Demeke, Ayele; Tegos, I.A., "Steel fiber reinforced concrete in biaxial stress tension-compression conditions," vol. 91, 1994.

[12] J.W. Schultze, M.M. Lohrengel, vol. 45, 2000.

[13] C. M. Hansson, "Comments on electrochemical measurements of the rate of corrosion of steel in concrete," Cement and Concrete Research, vol. 14, 1984.

[14] A. C. 222, Protection of Metals in Concrete against Corrosion, Michigan: ACI 222R-01, American Concrete Institute,Farmington Hills, 2001.

[15] V.N. Shah, C.J. Hookham., "Long-term aging of light water reactor concrete containments," vol. 185, 1998.

[16] M. F. Montemor, A. M. P. Simões, M. G. S. Ferreira, "Analytical Characterization of the Passive Film Formed on Steel in Solutions Simulating the Concrete Interstitial Electrolyte.," vol. 54, 1998.

[17] Bertolini L, Bolzoni F, Pastore T, Pedeferri P. , "Behaviour of stainless steel in simulated concrete pore solution," vol. 31, 1996.

[18] Bertolini L, Pedeferri P., "Laboratory and field experience on the use of stainless steel to improve durability of reinforced concrete.," vol. 20, 2002.

[19] H. Bruno, V.L. Hostis, F. Miserque, H. Idrissi, "Electrochemical behavior of mild steel in concrete: influence of PH and carbonate content of concrete pore solution," vol. 51, 2005.

[20] D. R. Lide, CRC Handbook of chemistry and physics, New York, NY: CRC press, 1999.

[21] S. Joiret, M. Keddam, X.R. Novoa, M.C. Perez, C. Rangel, H. Takenouti, "Use of EIS,ring-disk electrode, EQCM and Raman spectroscopy to study the film of oxides formed on iron in 1 M NaOH," vol. 24, 2002.

[22] Bard, Allen J., Larry R. Faulkner, Electrochemical Methods: Fundamentals and Applications, Wiley, 1980.

[23] S. R. Morrison, Electrochemistry at semiconductor and oxidized metal electrodes., New York: Plenum Press., 1981.

[24] H. H. Uhlig, " Corrosion and corrosion control : an introduction to corrosion science and engineering.," Wiley, 1985.

[25] A. M. Sukhotin, M. S. Grilikhes, and E. V. Lisovaya, " The influence of passivation on the kinetics of the dissolution of iron—I. Outer layer of the passivating film as a heavy doped thin semiconductor and M-S equation.," Electrochim. Acta, vol. 34, 1989.

[26] P. Schmuki, H. Böhni, and J. A. Bardwell, "In situ characterization of anodic silicon oxide films by AC impedance measurements," Journal of electroanalytical Society, vol. 142(5), pp. 1705-1712., 1995.

[27] A. D. Paola, "Semiconducting properties of passive films on stainless steels.," Electrochimica Acta, pp. 3-210., 1989.

[28] A. Simoes, M. Ferreira, B. Rondot, and M. Belo, " Study of passive films formed on AISI 304 stainless steel by impedance measurements and photoelectrochemistry.," Journal of Electrochemical Society, pp. 82-87., 1990.

[29] C. Sunseri, S. Piazza, A. Dipaola, and F. Diquarto, " A photocurrent spectroscopic investigation of passive films on ferritic stainless steels.," Journal of Electrochemical Society, pp. 2410-2416., 1987.

[30] P. Schmuki and H. Böhni, "Metastable pitting and semiconductive properties of passive films.," Journal of electroanalytical Society, pp. 1908-1913, 1992.

[31] M. Da Cunha Belo, N. E. Hakiki, and M.G.S. Ferreira, " Semiconducting properties of passive films formed on nickel–base alloys type Alloy 600: influence of the alloying elements.," Electrochimica Acta, pp. 2473-2481., 1999..

[32] A. Di Paola, F. Di Quarto, and C. Sunseri, , "A photoelectrochemical characterization of passive films on stainless steels.," Corrosion Science,, vol. 26, pp. 935-948., 1986..

[33] P. Ghods, " Multi-scale investigation of the formation and breakdown of passive films on carbon steel rebar in concrete.," PhD thesis in Civil Engineering, , Carlton University, 2010.

[34] P. Ghods, O. B. Isgor, G. McRae, and T. Miller, "The effect of concrete pore solution composition on the quality of passive oxide films on black steel reinforcement.," Cement and Concrete Composites, vol. 31, 2009.

[35] A. Di Paola and D. Shukla,, " Photoelectrochemical study of passive on stainless steel in neutral solutions.," Electrochim Acta, vol. 36, pp. 345-352., 1991.

[36] T. D. Burleigh and R. M. Latanision, " The use of photocurrents to characterize anodic films on Ti, Zr, Cu, and 304 stainless steel.," Journal of electroanalytical Society,, vol. 134, pp. 135-141., 1987. .

[37] J. A. Harrison and D. E. Williams, "How does the electrochemical behavior of stainless steel reflect that of its constituent elements.," Electrochimica Acta, vol. 31, pp. 1063-72., 1986. .

[38] A. W. Bott, " Electrochemistry of Semiconductors.," Current Separations, vol. 17, pp. 87-91., 1998..

[39] Ai Hongmei, Bai Junying, "Study on the Effect of Oxygen Ions on the Steel Corrosion in Concrete," in Communications and networks, International Conference, 2011.

[40] L. Xuean, "Cause of Steel Corrosion in Concrete and Its Prevention," vol. 7, 2009.

[41] W. Jun, "Reasons of steel corrosion and corrosion—resistance design in concrete," vol. 8, 2008.

[42] Arnon Bentur, Sidney Diamond, Neal Steven Berke, "Steel corrosion in concrete: fundamentals and civil engineering practice".

[43] J. P.Broomifield., "Corrosion of Steel in Concrete: understanding, investigation, and repair," E & FN Spon, an imprint of Chapman & Hall, 1997.

[44] J. Y. Zhang, "Corrosion of reinforcing steel in concrete structures: understanding the mechanisms," 2008.

[45] M. Saremi, E. Mahallati, "A study on chloride-induced depassivation of mild steel in simulated concrete pore solution," vol. 32, 2002.

[46] Z. Yun-lian, "Electrochemical study on semiconductive properties of the passive film on rebar in concrete," vol. 7, 2006.

[47] Clear, K.C., and Hay, R.E., "“Time-to-Corrosion of Reinforcing Steel in Concrete Slabe, V.1: Effect of Mix Design and Construction Parameters,” Report No. FHWA-RD-73-32," Federal Highway Administration, Washington, DC, 1973.

[48] C. K.C, "“Time-to-Corrosion of Reinforcing Steel in Concrete Slabs”," Federal Highway Administration, 1976.

[49] D. A. Jones, Principles and Prevention of Corrosion, Prentice Hall, 1995.

[50] Xiaodong Liu, G.S. Frankel., " Effect of applied tensile stress on intergranular corrosion of AA2024-T3," Corrosion Science, 2004.

[51] F.Navai, "Effects of tensile and compressive stresses on the passive layers formed on a type 302 stainless steel in a normal sulphuric acid bath," vol. 30, 1995.

[52] F.Navai, "Electrochemical behavior of a type 302 stainless steel in a stress field," vol. 23, 2000.

[53] S.J. Jaffer, C.M. Hansson, "Chloride-induced corrosion products of steel in cracked-concrete subjected to different loading conditions," vol. 39, 2009.

[54] Xingguo Feng, Yuming Tang, Yu Zuo, "Influence of stress on passive behaviour of steel bars in concrete pore solution," vol. 53, 2011.

[55] Poursaee. A., C.M. Hansson, "Reinforcing steel passivation in mortar and pore solution," vol. 37, 2007.

[56] ASTM standards Designation: G 39-99, Standard Practice for Preparation and Use of Bent-Beam Stress-Corrosion Test Specimens, ASTM.

[57] R.C.Hibbeler, Mechanics of Material.

[58] ASTM A179. SAE 1018 Steel Properties., ASTM.

[59] A. Poursaee, "Corrosion of steel bars in saturated Ca(OH)2 and concrete pore solution," vol. 1, 2010.

[60] Hansson, C.M., T. Frolund, and J.B. Markussen, "The effect of chloride cation type on the corrosion of steel in concrete by chloride salts," vol. 15, 1985.

[61] C. M. Hansson, A. Poursaee, and A. Laurent, "Macrocell and microcell corrosion of steel in ordinary Portland cement and high performance concretes," vol. 36, 2006.

[62] EC lab v10.18.

[63] ASTM C876-09, West Conshohocken, PA: ASTM International, 2009.

[64] M.Stern and .L.Geary J., "Electrochemical Polarisation: I: A theoretical Analysis of the Shape of Polarisation Curves," vol. 104, 1957.

[65] Andrade, C. and González, J. A., "Quantitative Measurements of Corrosion Rate of Reinforcing Steels Embedded in Concrete Using Polarization Resistance Measurements," vol. 29, 1978.

[66] Andrade, C., Marcias, A., Feliu, S., Escudero, M. L., and Gonzalez, J. A., "Quantitative Measurement of the Corrosion Rate Using a Small Counter Electrode in the Boundary of Passive and Corroded Zones of a Long Concrete Beam," 1990.

[67] A. Poursaee., " Corrosion Measurement Techniques in Steel Reinforced Concrete.," Journal of ASTM International, vol. Vol. 8.

[68] Silverman, D. C., R. Baboian and W. Dean, "Simple Models/Practical Answers," 1990.

[69] Lasia, A.,B. E. Conway, J. Bockris, and R. E. White,, "“Electrochemical Impedance Spectroscopy and its Applications,” Modern Aspects of Elec-trochemistry," 1999.

[70] Silverman, Density estimation for statistics and data analysis, 1986.

[71] Princeton Applied Research.

[72] Gamry Instruments, 2006.

[73] Myamlin, V. A., and Yu V. Pleskov., ""Electrochemistry of SemiconductorsPlenum."," Plenum Press, NY, 1967.

[74] Nozik AJ, Memming R., "Physical chemistry of semiconductor-liquid interfaces," The Journal of Physical Chemistry, 1996.

[75] N. F. Mott, "A theory of the formation of protective oxide films on metals," Transactions of the Faraday Society, vol. A, 1939.

[76] Schottky, W.,R. De Gryse, R. De Gryse,W. P. Gomes, F. Cardon and J. Vennik, 1975.

[77] W. John Albery, Gerald J. O'Shea and Alec L. Smith., "Interpretation and use of Mott-Schottky plots at the semiconductor/electrolyte interface," J. Chem. Soc., Faraday Trans, vol. 92, 1996.

[78] W. Kemula, Z. Kublik, "Application of the hanging mercury drop electrode to an investigation of intermetallic compounds in mercury," Nature, vol. 182, 1958.

[79] R.N.Adams, "Electrochemistry at Solid electrodes," Marcel Dekker, Inc, 1968.

[80] L. D. Burke and M. E.G. Lyons, "The formation and stability of hydrous oxide films on iron under potential cycling conditions in aqueous solution at high pH.," Journal of Electroanalytical Chemistry and Interfacial Electrochemistry, , vol. 198, p. 347–368, 1986..

[81] L. D. Burke and O.J. Murphy, " Growth of an electrochromic film on iron in base under potential cycling conditions," Journal of Electroanalytical Chemistry and Interfacial Electrochemistry,, vol. 109, p. 379–383., 1980.

[82] M .L. Mateo, T. Fernandez Otero, and D. J. Schiffrin, " Mechanism of enhancement of the corrosion of steel by alternating currents and electrocatalytic properties of cycled steel surfaces.," Journal of Applied Electrochemistry,vol. 20, pp. 26-31.1990.